





This is to certify that the  
thesis entitled  
An Analytical And Experimental  
Investigation Of The Elastodynamic Response  
Of A Class Of Intelligent Machinery

presented by

Vasudivan Sunappan

has been accepted towards fulfillment  
of the requirements for

M.S. degree in Mechanical Engineering

A handwritten signature in cursive script, reading "Dr. S. Thompson". The signature is written in dark ink and is positioned above a horizontal line.

Major professor

Date 5 Feb 1987



RETURNING MATERIALS:

Place in book drop to  
remove this checkout from  
your record. FINES will  
be charged if book is  
returned after the date  
stamped below.

CX A 052

MAR 29 1960

CX 121

AN ANALYTICAL AND EXPERIMENTAL INVESTIGATION  
OF THE ELASTODYNAMIC RESPONSE OF A  
CLASS OF INTELLIGENT MACHINERY

By

Vasudivan Sunappan

A THESIS

Submitted to  
Michigan State University  
in partial fulfillment of the requirements  
for the degree of

MASTER OF SCIENCE

Department of Mechanical Engineering

1987



## **ABSTRACT**

# **AN ANALYTICAL AND EXPERIMENTAL INVESTIGATION OF THE ELASTODYNAMIC RESPONSE OF A CLASS OF INTELLIGENT MACHINERY**

By

VASUDIVAN SUNAPPAN

A methodology is proposed, herein, for reducing the elastodynamic response of high-speed machine systems by introducing an additional perturbational input which is computer-controlled. The work presented here describes a comprehensive analytical and experimental investigation on a bread-board model of the concept, in which the objective is to reduce the vibrational response at the midspan of a flexible rocker link of a "retrofitted" four-bar linkage. A variational formulation is employed to develop the equation governing the response of the flexible member to the combined parametric and forcing functions. This equation is then solved numerically and the viability of the model is validated by comparing the analytical results with response-data from a complementary experimental program. The stability of motion is examined using the above equation.

## ACKNOWLEDGMENTS

I wish to express my deepest gratitude to my advisor Dr. Brian S. Thompson for his guidance and assistance throughout this study and in preparation of this manuscript. His academic excellence and research philosophy have provided a constant source of encouragement.

I also wish to thank the members of my committee Dr. B. Fallahi and Dr. Steven W. Shaw for their helpful suggestions.

The efforts and assistance of Dr. C. K. Sung and K. M. Soong at Michigan State University are sincerely appreciated.

Finally, I would like to thank my parents for their encouragement and financial support that help to complete this work.

## TABLE OF CONTENTS

	page
List of Figures.....	v
Chapter 1. Introduction.....	1
1-1 Current Trends in Industrial Machinery.....	1
1-2 Intelligent Machine Systems.....	3
Chapter 2. Kinematic Analysis of The Modified Linkage.....	6
2-1 Introduction.....	6
2-2 Kinematics.....	7
2-3 Dynamics.....	12
Chapter 3. Variational Theorem.....	14
3-1 Theoretical Development.....	14
3-2 Approximations For The Variables.....	20
3-3 Construction of The Problem Definition.....	25
3-4 An Approximate Solution.....	30
Chapter 4. Solution to Hill's Equation.....	35
4-1 Quasi-Static Response.....	35
4-1 Elastodynamic Response.....	36
Chapter 5. Experimental Investigation.....	40
5-1 Experimental Apparatus.....	40
5-2 Instrumentation.....	44
5-3 Experimental Procedure.....	49
Chapter 6. Stability Analysis.....	53
6-1 Stability of Motion.....	53



Chapter 7.	Elastodynamic Response Of The Unmodified Linkage and The Synthesis Of The Shaker/Slider Motion.....	56
7-1	Response Curves for The Flexible Four-Bar Linkage...	56
7-2	Curve Synthesis for Shaker/Slider Motion.....	60
Chapter 8.	Experimental and Computational Results.....	72
8-1	Response Data and Absolute Acceleration of The Flexible Link.....	72
8-2	Kinematic Results of The Flexible Link.....	81
Chapter 9.	Discussion of Results.....	89
Chapter 10.	Conclusions.....	93
Chapter 11.	Future Work.....	94
Bibliography.....		95

## LIST OF FIGURES

Figure	page
2.1 Intelligent Mechanism:the kinematic chain.....	6
2.2 Vector-Loop Diagram.....	7
2.3 Component Pin Forces.....	11
3.1 Definition of axis systems and position vectors.....	14
3.2 The modelling of an Intelligent mechanism.....	21
3.3 Forces exerted at the rocker-slider pin joint.....	24
5.1 Experimental Intelligent Mechanism.....	41
5.2 Electrodynamic Shaker-Slider Assembly.....	41
5.3 Schematic Diagram of the Instrumentation.....	45
5.4 Assembly of Crank and Airpax pickup.....	46
5.5 Data-Acquisition System and Equipment.....	46
5.6 Transient Response of Rocker Link.....	49
5.7 Frequency-response curves for the four-bar linkage.....	51
5.8 Link Calibration-Fixation.....	52
6.1 Analytical Frequency-response curves.....	55
7.1 Elastodynamic Response of the Four-bar Linkage at 148 rpm.....	57
7.2 Elastodynamic Response of the Four-bar Linkage at 170 rpm.....	58
7.3 Elastodynamic Response of the Four-bar Linkage at 200 rpm.....	58
7.4 Elastodynamic Response of the Four-bar Linkage at 215 rpm.....	59
7.5 Quasi-static Response of the Four-bar Linkage at 200 rpm.....	59
7.6 Absolute Acceleration of The Rocker Link.....	63
7.7 Suggested shaker/slider waveform proportional to quasi-static response.....	65
7.8 Absolute acceleration of the rocker link at 200 rpm given shaker/slider waveform shown in Fig. 7.7.....	65

7.9	Analytical elastodynamic response at 200 rpm given shaker/slider waveform shown in Fig. 7.7.....	66
7.10	Experimental elastodynamic response at 200 rpm given shaker/slider waveform shown in Fig. 7.7.....	66
7.11	Angular acceleration of the rocker link at 200 rpm given shaker/slider waveform shown in Fig. 7.7.....	67
7.12	Suggested shaker/slider waveform inverse of quasi-static response.....	67
7.13	Absolute acceleration of the rocker link at 200 rpm given shaker/slider waveform shown in Fig. 7.12.....	68
7.14	Analytical elastodynamic response at 200 rpm given shaker/slider waveform shown in Fig. 7.12.....	68
7.15	Experimental elastodynamic response at 200 rpm given shaker/slider waveform shown in Fig. 7.12.....	69
7.16	Angular acceleration of the rocker link at 200 rpm given shaker/slider waveform shown in Fig. 7.12.....	69
7.17	Synthesis of shaker/slider waveform.....	71
8.1	Experimental elastodynamic response at 148 rpm.....	73
8.2	Experimental quasi-static response at 148 rpm.....	73
8.3	Analytical elastodynamic response at 148 rpm.....	74
8.4	Analytical quasi-static response at 148 rpm.....	74
8.5	Absolute acceleration of the rocker link at 148 rpm.....	75
8.6	Experimental elastodynamic response at 170 rpm.....	75
8.7	Analytical elastodynamic response at 170 rpm.....	76
8.8	Absolute acceleration of the rocker link at 170 rpm.....	76
8.9	Experimental elastodynamic response at 200 rpm.....	77
8.10	Analytical elastodynamic response at 200 rpm.....	77
8.11	Absolute acceleration of the rocker link at 200 rpm.....	78
8.12	Analytical and experimental results for the intelligent mechanism at 200 rpm.....	78
8.13	Experimental elastodynamic response at 215 rpm.....	79
8.14	Experimental quasi-static response at 215 rpm.....	79
8.15	Analytical elastodynamic response at 215 rpm.....	80

8.16	Absolute acceleration of the rocker link at 215 rpm.....	80
8.17	Shaker/slider displacement at 148 rpm.....	82
8.18	Shaker/slider displacement at 170 rpm.....	82
8.19	Shaker/slider displacement at 200 rpm.....	82
8.20	Shaker/slider displacement at 215 rpm.....	83
8.21	Shaker/slider velocity at 148 rpm.....	83
8.22	Shaker/slider velocity at 170 rpm.....	83
8.23	Shaker/slider velocity at 200 rpm.....	84
8.24	Shaker/slider velocity at 215 rpm.....	84
8.25	Shaker/slider acceleration at 148 rpm.....	84
8.26	Shaker/slider acceleration at 170 rpm.....	85
8.27	Shaker/slider acceleration at 200 rpm.....	85
8.28	Shaker/slider acceleration at 215 rpm.....	85
8.29	Force exerted by the shaker on the slider at 148 rpm.....	86
8.30	Force exerted by the shaker on the slider at 170 rpm.....	86
8.31	Force exerted by the shaker on the slider at 200 rpm.....	86
8.32	Force exerted by the shaker on the slider at 215 rpm.....	87
8.33	Angular acceleration of the rocker link at 148 rpm.....	87
8.34	Angular acceleration of the rocker link at 170 rpm.....	87
8.35	Angular acceleration of the rocker link at 200 rpm.....	88
8.36	Angular acceleration of the rocker link at 215 rpm.....	88

## **CHAPTER 1**

### **INTRODUCTION**

#### **1-1 CURRENT TRENDS IN INDUSTRIAL MACHINERY**

The intense competition in the international marketplace for robots and machine systems which significantly enhance manufacturing productivity by operating at high speeds has resulted in the evolution of a new frontier in machine design. Under these more stringent operating conditions, the traditional design methodologies are unable to adequately predict a machine's performance because elastodynamic phenomena are stimulated due to the inherent flexibility of the moving parts. The traditional design methodologies are based on dynamic analyses wherein all mechanism members are treated as rigid-bodies.

When operating in a high-speed mode, vibrations and dynamic stresses in the members of a mechanism can drastically modify the performance characteristics, and the fatigue-life of parts becomes a significant design consideration. Furthermore, the radial clearances in sleeve bearings in mechanical and electro-mechanical systems, which are essential for the operation of these joints, will generally result in excessive stresses and impact loads, and these loads can generate more severe problems such as wear, loss of performance, increased levels of noise and vibration.

The trend towards ultra-high operating speeds as a method for increasing productivity has exacerbated the design of modern machine systems and as a consequence of these stimuli, the research community

has responded by developing more sophisticated modeling techniques [1,2,3]. In addition to these enhanced predictive capabilities, described in the above review articles the academic community has also developed two design methodologies for reducing the elastodynamic response of linkage machinery. (Vibrations or deflections in a mechanism with elastic links under dynamic conditions is called elastodynamic response.) The first advocates that the articulating members of these mechanical systems should be designed with optimal cross-sectional geometries and fabricated from commercial metals [4,5,6,7,8]. The second advocates that the articulating members should be designed with polymeric composite laminates which are optimally-tailored in order to synthesize the material properties for the specific application [9,10,11,12]. When implemented, the foregoing methodologies achieve a reduction in the levels of the dynamic response by increasing the stiffness/weight ratios of the members by tailoring both the geometrical and material properties of the articulating members.

The rationale can be clarified by examining the terms in the approximate linear finite element equations governing the elastodynamic response of a general machine system presented below,

$$[M]^{-1}[K]\{U\} + [M]^{-1}[C]\{\dot{U}\} + [I]\{\ddot{U}\} = -[I]\{R\} \quad (1.1)$$

where  $[M]$ ,  $[K]$  and  $[C]$  are the global mass, stiffness and damping matrices respectively of the system,  $[I]$  is the identity matrix,  $\{U\}$  represents the discretized deformation field, the overdot denotes the time derivative and  $\{R\}$  represents the discretized rigid-body acceleration field. Thus for a prescribed machine system operating at a

prescribed speed the elastodynamic response is principally dictated by the stiffness-to-mass ratio of the links.

In contrast to the foregoing methodologies which focus on the mass and stiffness terms on the left-hand-side of equation (1.1), the methodology proposed herein focuses on the right-hand-side of equation (1.1); namely the kinematic variables which provide the principal system excitation in a high-speed mode of operation. Thus it is argued, if the magnitude of these variables, and hence the inertial loading, can be reduced, then so too will the elastodynamic response. This translates into a reduction in the dynamic deflections of articulating members, a reduction in the associated dynamic stresses, and also a reduction in the severity of the fatigue environment in which the members must operate.

## 1-2 INTELLIGENT MACHINE SYSTEMS

Intelligent machine systems have been the subject of numerous publications, principally in the context of robotic manipulators [13,14], but of course this terminology really pertains to a very broad spectrum of machine products which incorporates sensors and computers. The research reported, herein addresses intelligent machinery in this broader context, by proposing a general methodology for controlling the elastodynamic response of linkages machinery.

The current generation of robotic and intelligent machine systems are capable of undertaking many diverse tasks, and implicit in this statement is embedded a spectrum of diverse technologies from several

different disciplines, such as instrumentation, controls, computing, artificial intelligence, materials and machine dynamics.

In contrast to these robotic-orientated publications, herein, the focus of attention is the attenuation of the elastodynamic response of flexible linkage machinery which feature in a very broad range of both industrial and commercial machinery and equipment. These classes of mechanism systems are prone to generate a vibrational response when operating in a high-speed mode, which is attributed to the time-dependent inertial loading imposed upon the members of the articulating system, since these members are inherently an assemblage of flexible, not rigid bodies. Typical contributions to this field include references [15].

The objective, herein, is to develop and then experimentally test the viability of a methodology for reducing the response of flexible members of linkage mechanisms by introducing an additional input in the kinematic chain. The concept is evaluated by studying a bread-board model of the proposed approach which comprises a retrofitted planar four-bar linkage with a flexible rocker link. The retrofitment involves modifying the normally stationary ground-link/rocker-link revolute joint to incorporate an additional prismatic joint whose perturbational motion is controlled by an electrodynamic shaker which is driven by an arbitrary waveform/function generator. The linkage can function as a classical four-bar mechanism by locking the prismatic joint, or alternatively, as a five-bar linkage by releasing this locking device. In this latter mode, the system has two nominally rigid-body degrees of freedom with inputs provided by the crank rotation and also the motion



of the shaker. The idea was first reported in a theoretical publication [16] prior to presenting some preliminary experimental work in reference [17].

The equations of motion and the relevant boundary conditions for the flexible rocker link are derived using a variational technique, and the steady-state response is obtained using an approach developed by Hsu [18]. An analysis of the corresponding homogeneous equation is developed by means of which the stability of motion are examined. The computational results correlate favorably with experimental data from a complementary experimental investigation.

## CHAPTER 2

### KINEMATIC ANALYSIS OF THE MODIFIED LINKAGE

#### 2-1 INTRODUCTION

The kinematic characteristics of the rocker link need to be evaluated prior to determining the midspan transverse deflection. The kinematics of a four-bar linkage have been investigated widely, but for the intelligent mechanism, the kinematic analysis of a four-bar linkage with two-degrees of freedom is necessary. The kinematics of this linkage are evaluated assuming the links are rigid, and the effects of friction and clearance at the bearings are neglected. The kinematic analysis of four-bar linkage found in reference [19] is modified in order to analyze the proposed class of intelligent mechanism.

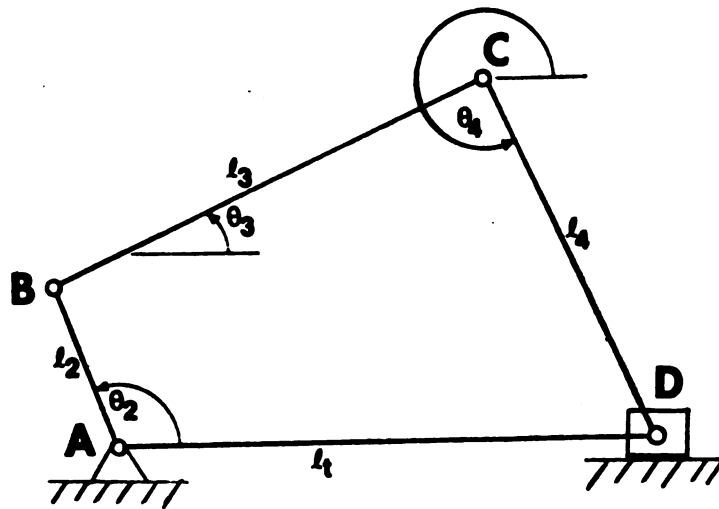


Fig. 2.1 : Intelligent Mechanism:the kinematic chain

The linkage under consideration is shown in Fig. 2.1, where  $l_t$  is the length of ground link which is variable with time and  $l_2$ ,  $l_3$  and  $l_4$  are the lengths of the crank AB, coupler BC and rocker CD respectively. The angles  $\theta_2$ ,  $\theta_3$ , and  $\theta_4$  are the angles of each link. The corresponding angular velocities and angular accelerations are denoted by  $\omega_2$ ,  $\omega_3$ ,  $\omega_4$  and  $\alpha_2$ ,  $\alpha_3$ ,  $\alpha_4$  respectively. For the intelligent mechanism,  $\omega_2$  is constant and hence  $\alpha_2 = 0$ .

## 2-2 KINEMATICS

### 2-2.1 VECTOR ANALYSIS

If  $\vec{l}_t$ ,  $\vec{l}_2$ ,  $\vec{l}_3$  and  $\vec{l}_4$  represent the vectors AD, AB, BC and CD respectively, it follows from Fig. 2.2 that

$$\vec{l}_2 + \vec{l}_3 + \vec{l}_4 = \vec{l}_t \quad (2.1)$$

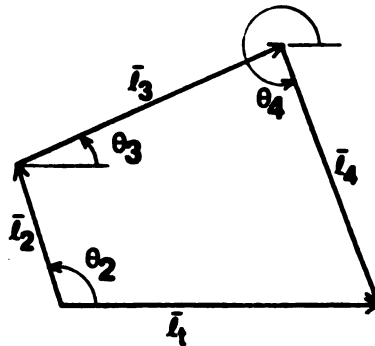


Fig. 2.2 : Vector-Loop Diagram

and by writing  $\vec{l}_r = l_r e^{i\theta_r}$  ( $r = 1, 2, 3, 4$ ) in complex number notation, equation (2.1) becomes

$$l_2 e^{i\theta_2} + l_3 e^{i\theta_3} + l_4 e^{i\theta_4} = l_t e^{i\theta_1} \quad (2.2)$$

where  $\theta_1 = 0$  from Fig. 2.2

### 2-2.2 POSITION ANALYSIS

The Euler equation ( $e^{i\theta} = \cos\theta + i\sin\theta$ ) is substituted into eq. (2.2) prior to separating the real and imaginary parts. This process yield equations for the angular positions of the coupler and rocker links in terms of the input angle of the crank. They are

$$l_2 \cos\theta_2 + l_3 \cos\theta_3 + l_4 \cos\theta_4 = l_t \quad (2.3a)$$

$$l_2 \sin\theta_2 + l_3 \sin\theta_3 + l_4 \sin\theta_4 = 0 \quad (2.3b)$$

Solving equation (2.3) for  $\cos\theta_3$ , yields the expression

$$\cos\theta_3 = \frac{AB}{D} \pm \left[ \left( \frac{AB}{D} \right)^2 - \frac{B^2 - C^2}{D^2} \right]^{1/2} \quad (2.4)$$

where

$$A = 2l_3(l_2 \cos\theta_2 - l_t)$$

$$B = l_4^2 - l_t^2 - l_2^2 - l_3^2 + 2l_t l_2 \cos \theta_2$$

$$C = 2l_2 l_3 \sin \theta_2$$

$$D = (A^2 + C^2)^{1/2}$$

Once  $\theta_3$  has been determined from equation (2.4), the value of  $\theta_4$  follows from eq. (2.3)

### 2-2.3 ANGULAR VELOCITIES

Upon differentiating (2.2) with respect to time and separating real and imaginary parts and solving for  $\omega_3$  and  $\omega_4$  yields

$$\omega_3 = - \frac{l_2 \omega_2 \sin(\theta_2 - \theta_4) + l_t \cos \theta_4}{l_3 \sin(\theta_3 - \theta_4)} \quad (2.5a)$$

$$\omega_4 = - \frac{l_2 \omega_2 \sin(\theta_2 - \theta_3) + l_t \cos \theta_3}{l_4 \sin(\theta_4 - \theta_3)} \quad (2.5b)$$

### 2-2.4 ANGULAR ACCELERATIONS

The angular acceleration of the coupler and the rocker may be obtained by differentiating (2.2) twice with respect to time and separating the real and imaginary parts. The results can be expressed in the form

$$\alpha_3 = - \frac{l_2 \omega_2^2 \cos(\theta_4 - \theta_2) + l_3 \omega_2^2 \cos(\theta_4 - \theta_3) + l_4 \omega_2^2 + \ddot{l}_t \cos \theta_4}{l_3 \sin(\theta_3 - \theta_4)} \quad (2.6a)$$

$$\alpha_4 = - \frac{l_2 \omega_2^2 \cos(\theta_3 - \theta_2) + l_4 \omega_4^2 \cos(\theta_3 - \theta_4) + l_3 \omega_3^2 + \ddot{l}_t \cos \theta_3}{l_4 \sin(\theta_4 - \theta_3)} \quad (2.6b)$$

### 2-2.5 LINEAR ACCELERATIONS

Expressions for the linear accelerations of the centers of mass  $G_2$ ,  $G_3$ , and  $G_4$  of the moving links follow from the preceding equations. The expressions are written according to the coordinate axes shown in Fig. 2.3. Thus, if  $AG_2 = r_2$ ,  $BG_3 = r_3$  and  $DG_4 = r_4$ , the component accelerations are written as  $(a_{2x}, a_{2y})$ ,  $(a_{3x}, a_{3y})$  and  $(a_{4x}, a_{4y})$  and can be expressed as

$$a_{2x} = -r_2(\omega_2^2 \cos \theta_2 + \alpha_2 \sin \theta_2) \quad (2.7a)$$

$$a_{2y} = -r_2(\omega_2^2 \sin \theta_2 - \alpha_2 \cos \theta_2) \quad (2.7b)$$

$$a_{3x} = (l_2/r_2)a_{2x} - r_3(\omega_3^2 \cos \theta_3 + \alpha_3 \sin \theta_3) \quad (2.7c)$$

$$a_{3y} = (l_2/r_2)a_{2y} - r_3(\omega_3^2 \sin \theta_3 - \alpha_3 \cos \theta_3) \quad (2.7d)$$

$$a_{4x} = \ddot{l}_t - r_4(\alpha_4 \sin \theta_4' + \omega_4^2 \cos \theta_4') \quad (2.7e)$$

$$a_{4y} = -r_4(\omega_4^2 \sin \theta_4' - \alpha_4 \cos \theta_4') \quad (2.7f)$$

where  $\theta_4' = (\theta_4 - \pi)$

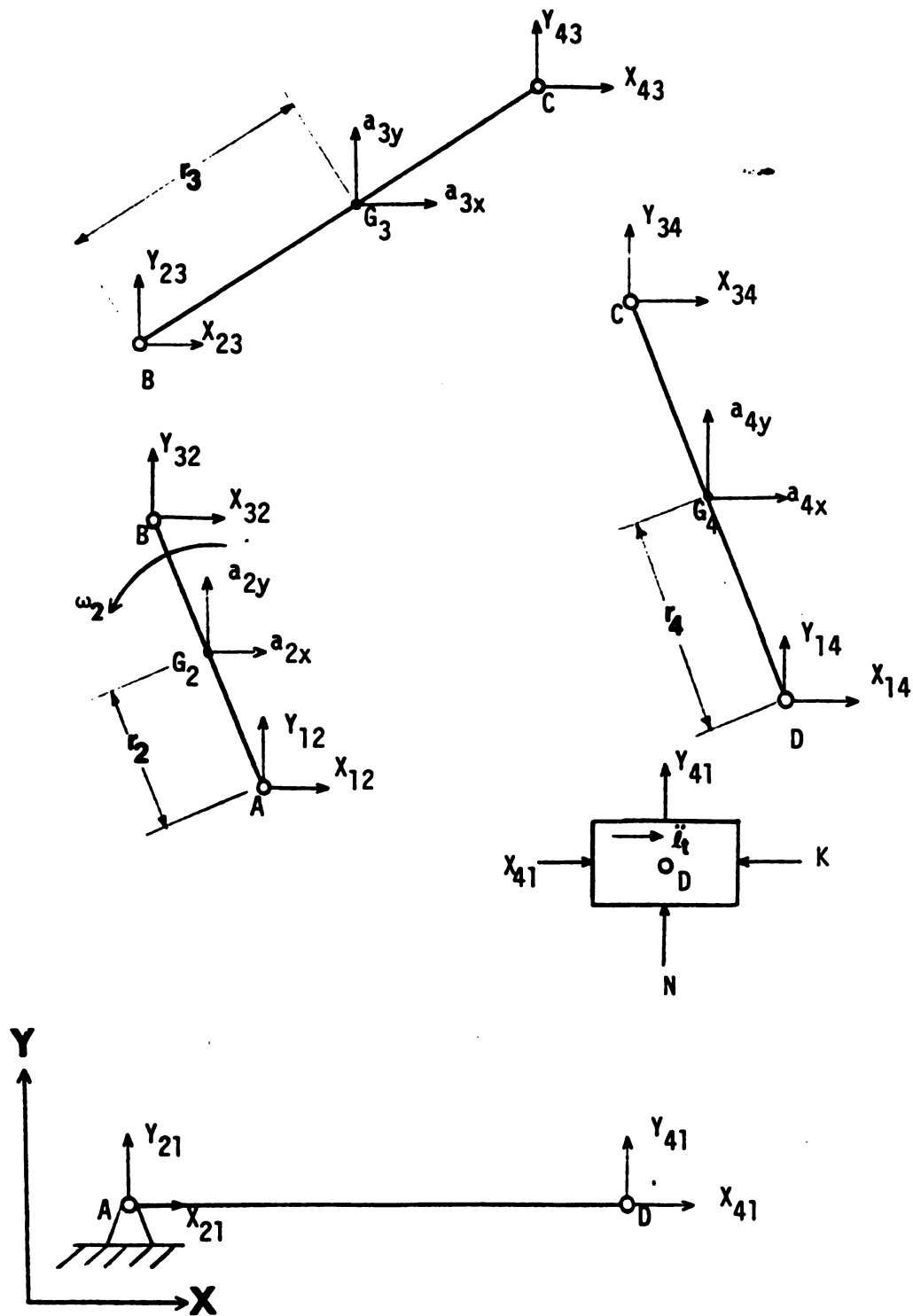


Fig. 2.3 : Component Pin Forces

## 2-3 DYNAMICS

The forces acting at the joints of the mechanism is shown in Fig. 2.3, where, for example,  $X_{14}$  represents the component of the force exerted by link 1 on link 4. Thus  $X_{14} = -X_{41}$  and etc.  $N$  is the normal force exerted by the slider guide on the slider and the force exerted by the shaker is denoted by  $K$ . The slider acceleration  $\ddot{l}_t$  is in the  $OX$  direction.

The notations  $m_2$ ,  $m_3$  and  $m_4$  are the masses of the links and  $I_{2A}$ ,  $I_{3B}$  and  $I_{4D}$  are the corresponding moments of inertia about axes perpendicular to the plane of motion and passing through points A, B and D respectively. Then, the equations of motion necessary to evaluate the forces acting on the rocker link are

$$X_{23} - X_{34} = m_3 a_{3x} \quad (2.8a)$$

$$Y_{23} - Y_{34} = m_3 a_{3y} \quad (2.8b)$$

$$X_{34} - X_{41} = m_4 a_{4x} \quad (2.8c)$$

$$Y_{34} - Y_{41} = m_4 a_{4y} \quad (2.8d)$$

$$\begin{aligned} X_{23}r_3\sin\theta_3 - Y_{23}r_3\cos\theta_3 + X_{34}(\ell_3 - r_3)\sin\theta_3 \\ - Y_{34}(\ell_3 - r_3)\cos\theta_3 = (I_{3B} - m_3 r_3^2)\alpha_3 \end{aligned} \quad (2.8e)$$

$$- X_{34}\ell_4\sin(\theta_4 - \pi) + Y_{34}\ell_4\cos\theta_4' = I_{4D}\alpha_4 \quad (2.8f)$$



Solving the above equations for the pin forces yields the following expressions,

$$X_{34} = \frac{I_{3B}\alpha_3 l_4 \cos\theta_4' + I_{4D}\alpha_4 l_3 \cos\theta_3 - \omega_2^2 m_3 r_3 l_2 l_4 \cos\theta_4' \sin(\theta_2 - \theta_3)}{l_3 l_4 \sin(\theta_3 - \theta_4')} \quad (2.9a)$$

$$Y_{34} = \frac{I_{3B}\alpha_3 l_4 \sin\theta_4' + I_{4D}\alpha_4 l_3 \sin\theta_3 - \omega_2^2 m_3 r_3 l_2 l_4 \sin\theta_4' \sin(\theta_2 - \theta_3)}{l_3 l_4 \sin(\theta_3 - \theta_4')} \quad (2.9b)$$

$$X_{41} = X_{34} - m_4 a_{4x} \quad (2.9c)$$

$$Y_{41} = Y_{34} - m_4 a_{4y} \quad (2.9d)$$

The force exerted by the slider guide and the shaker is given by

$$N = -Y_{41} \quad (2.10a)$$

$$K = X_{41} - M_s \ddot{l}_t \quad (2.10b)$$

where  $M_s$  is the mass of the slider.

## CHAPTER 3

### VARIATIONAL THEOREM

The objective of this chapter is to develop the equations of motion governing the elastic rocker link. An accurate mathematical model is required which will accommodate the inherent elastic deformations of the link. The variational theorem forming the kernel of this theoretical study was originally developed in the doctoral dissertation of B.S. Thompson [20]. It incorporates the geometrically non-linear form of the field equations so that it may provide a basis for analysing linkages susceptible to dynamic instabilities and also mechanism systems that must be analysed using higher-order theories.

#### 3-1 THEORETICAL DEVELOPMENT

The theoretical development follows the approach of reference [21]. The dynamical problem of an elastic body describing a general

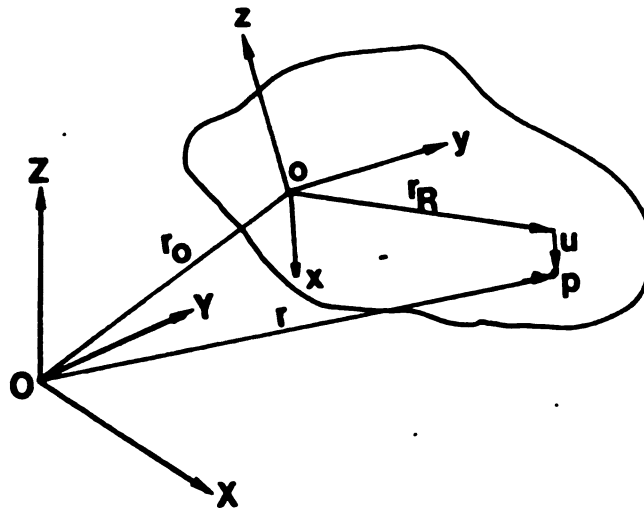


Fig. 3.1 : Definition of axis systems and position vectors

spatial motion relative to an inertial reference frame is considered. In Fig. 3.1, axes OXYZ define the inertial reference frame, while oxyz are Lagrangian coordinates fixed in the body in a reference state containing zero stresses and strains. Employing an indicial notation (i-x,y,z), then at time t, a general point P in the continuum has the position vector  $r_i$ , which is defined as

$$r_i = r_{oi} + r_{Ri} + u_i \quad (3.1)$$

where

$r_{oi}$  : the component relative to o-x-y-z frame of the position vector of the origin of the body axes relative to the origin of the inertial frame

$r_{Ri}$  : the position vector of point P in the reference state relative to the origin of the body axes

$u_i$  : the deformation displacement vector

The non-linear form of the field equations necessary for a body describing a general spatial motion relative to OXYZ frame are as follows:

$$(1) \quad p_i = \dot{r}_{oi} + \dot{u}_i + \epsilon_{ijk} \dot{\phi}_j (r_{ok} + r_{Rk} + u_k) \quad (3.2)$$

This equation is obtained by differentiating eq. (3.1)

where

$p_i$  : the velocity associated with the time rate of  $r_i$

$\epsilon_{ijk}$  : alternating tensor

$\phi_j$  : component of angular velocity vector for the moving axes or  
Lagrangian frame

$(\sim)$  : the time rate of change with respect to the moving frame

$(\bullet)$  : the absolute rate of change with respect to time

(ii) The boundary conditions for prescribed surface tractions and deformation displacements are written as

$$\bar{g}_i \quad \text{on } S_1 \quad (3.3)$$

$$\bar{u}_i = u_i \quad \text{on } S_2$$

where

$S_1$  : surface on which the prescribed tractions are imposed

$S_2$  : surface on which the prescribed displacements are imposed

(iii) Non-linear strain-displacement relations

$$\gamma_{ij} = \frac{1}{2}(u_{i,j} + u_{j,i} + u_{k,i}u_{k,j}) \quad (3.4)$$

where

$\gamma_{ij}$  : Lagrangian strain component

$(,)$  : denotes spatial differentiation

The kinetic energy density  $T$ , of the system is defined as

$$T = \frac{1}{2} \rho \delta_{ij} p_i p_j \quad (3.5)$$

where

$\rho$  : the mass density of the material

$\delta_{ij}$  : the kronecker delta

Further, defining  $W$  as the strain-energy density and  $X_i$  as the body forces per unit volume, the principle of virtual work leads to the problem of determining the stationary conditions of the functional

$$G = \int_{t_0}^{t_1} \left\{ \int_V [T(p_i) - W(\gamma_{ij}) + X_i r_i] dV + \int_{S_1} \bar{g}_i r_i dS \right\} dt \quad (3.6)$$

subject to the auxiliary conditions through the volume and over the surface  $S_2$ , the prescribed deformation displacement condition. The volume integral extends over the entire volume  $V$  of the elastic body and sum of  $S_1$  and  $S_2$  defines the total surface area  $S$  of the continuum.

A free variation problem without auxiliary conditions may be constructed by the Lagrange multiplier method which incorporates the constraints in the functional. The first variation of the modified functional enables these undetermined multipliers to be expressed in terms of the system parameters [21]. To obtain this expression it is necessary to use Gauss' theorem relating surface and volume integrals, and to perform integration by parts. Furthermore no variation in the system configuration is permitted at  $t_0$  and  $t_1$ .

The variations in the position vector  $r_i$  is obtained by permitting the variations to coincide with the actual displacement that occur during the time interval  $dt$ . The following relationship may be proved

$$\delta r_i = \delta r_{oi} + e_{ijk} \delta \phi_j (r_{ok} + r_{Rk} + u_k) \quad (3.7)$$

The functional becomes

$$\begin{aligned} J = & \int_{t_0}^{t_1} \left\{ \int_V (T(p_i) - W(\gamma_{ij}) + X_i r_i + r_{ij} [\gamma_{ij} - \frac{1}{2}(u_{i,j} + u_{j,i} + u_{k,i} u_{k,j})] \right. \\ & - \rho p_i [p_i - (\tilde{r}_{oi} + \tilde{u}_i + e_{ijk} \phi_j (r_{ok} + r_{Rk} + u_k))] ) dV \\ & \left. + \int_{s_1} \bar{g}_i r_i dS - \int_{s_2} (g_i + u_{i,k} g_k) (\bar{u}_i - u_i) dS \right\} dt \quad (3.8) \end{aligned}$$

The first variation must vanish for stationary conditions and the corresponding variational equation is

$$\begin{aligned} \delta J = 0 = & \int_{t_0}^{t_1} \left\{ \int_V \delta \gamma_{ij} [r_{ij} - (\partial W / \partial \gamma_{ij})] dV + \int_V \delta r_{ij} [\gamma_{ij} - \frac{1}{2}(u_{i,j} + u_{j,i} + u_{k,i} u_{k,j})] dV \right. \\ & - \int_V \rho \delta p_i [p_i - (\tilde{r}_{oi} + \tilde{u}_i + e_{ijk} \phi_j (r_{ok} + r_{Rk} + u_k))] dV \quad (3.9) \\ & + \int_V \delta u_i [X_i + r_{ij,j} + u_{i,k} r_{jk} + u_{i,k} r_{jk,j} - \rho \dot{p}] dV \\ & \left. + \int_{s_1} \delta u_i (\bar{g}_i - g_i - u_{i,k} g_k) dS - \int_{s_2} (\delta g_i + \delta u_{i,k} g_k + u_{i,k} \delta g_k) (\bar{u}_i - u_i) dS \right\} \end{aligned}$$

$$\begin{aligned}
& + \delta \phi_j \left( \int_V e_{ijk} X_i (r_{ok} + r_{Rk} + u_k) dV + \int_{S_2} e_{ijk} \bar{g}_i (r_{ok} + r_{Rk} + u_k) dS \right. \\
& \left. - \int_V e_{ijk} \rho \dot{p}_i (r_{ok} + r_{Rk} + u_k) dV \right) + \delta r_{oi} \left( \int_V X_i dV + \int_{S_1} \bar{g}_i dS - \int \rho \dot{p}_i dV \right) \Bigg\} dt
\end{aligned}$$

where  $r_{ij}$  is the stress tensor.

If arbitrary variations of the system parameters  $p_i$ ,  $u_i$ ,  $r_{oi}$ ,  $r_{Ri}$ ,  $\gamma_{ij}$ ,  $r_{ij}$ ,  $\phi_j$  in eq. (3.9) are permitted, the characteristic equations for this class of elastodynamic problem follow and are the balance of linear and angular momentum for the complete continuum, the field equations defining the relationships between the velocity and rate of change of position, the stress-strain relations, the strain-displacement relations and the equations of equilibrium, subject to prescribed boundary conditions on region  $S_1$  and  $S_2$ .

The stationary conditions for the functional are obtained by solving the mixed boundary-value problem defined by eq. (3.9). Approximations such as the Euler-Bernoulli beam theory may be introduced since the flexible link is considered slender and the deformations small. This permits an approximate problem definition to be generated systematically. This will lead to approximate partial differential equations of motion with dependent variables in space and time.

Since the investigation focusses on the flexible link, the rigid-body equations of motion are of no interest, they may be removed from

the variational equation by assuming that the variations  $\delta\phi_j$  and  $\delta r_{oi}$ , which are arbitrary - are zero. Hence the final form of variational equation of motion is

$$\begin{aligned}
 \delta J = 0 = & \int_{t_0}^{t_1} \left\{ \int_V \delta \gamma_{ij} [\tau_{ij} - (\partial W / \partial \gamma_{ij})] dV + \int_V \delta \tau_{ij} [\gamma_{ij} - \frac{1}{2}(u_{i,j} + u_{j,i} + u_{k,i} + u_{k,j})] dV \right. \\
 & - \int_V \rho \delta p_i [p_i - (\tilde{r}_{oi} + \tilde{u}_i + e_{ijk} \phi_j (r_{ok} + r_{Rk} + u_k))] dV \\
 & + \int_V \delta u_i [X_i + r_{ij,j} + u_{i,k} \tau_{jk} + u_{i,k} \tau_{jk,j} - \rho \dot{p}] dV \\
 & \left. + \int_{s_1} \delta u_i (\bar{g}_i - g_i - u_{i,k} g_k) dS - \int_{s_2} (\delta g_i + \delta u_{i,k} g_k + u_{i,k} \delta g_k) (\bar{u}_i - u_i) dS \right\} dt
 \end{aligned} \quad (3.10)$$

### 3-2 APPROXIMATIONS FOR THE VARIABLES

Approximating statements for the system variables in eq. (3.10) must be formulated so that it may be used to construct the problem definition. The intelligent mechanism in Fig. 3.2 is assumed to have a rigid crank AB which rotates at constant speed  $\omega_2 (\omega_2 = \dot{\theta}_2)$ , rigid coupler BC and elastic rocker link CD of undeformed length L with a cross-sectional area A. The ground-link/rocker-link revolute joint is being harmonically excited in the horizontal direction OX while the crank foundation is grounded. The length  $\ell_c$  is variable with time. Smooth pin joints are assumed and the slider of the shaker translates in a frictionless guide. Coordinates ox yz are Lagrangian axes fixed in the rocker link in an undeformed reference state which is defined by



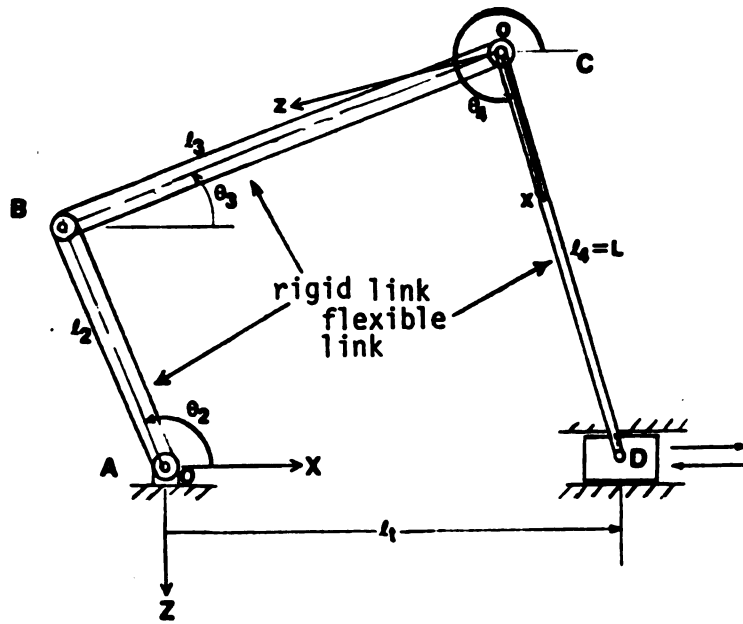


Fig. 3.2 : The modelling of an intelligent mechanism

the angle  $\theta_4$  relative to an inertial reference frame OXYZ. Approximation for the variables found in reference [22] is used here.

Deformation of the rocker link is restricted to simple axial and out of plane flexural components. If the link is considered slender and the deformations small, then the Euler-Bernoulli beam theory may be used and assumptions are

$$\begin{aligned} u_x &= u_o(x, t) - zw_{,x} \\ u_y &= 0 \\ u_z &= w(x, t) \end{aligned} \tag{3.11}$$

The longitudinal stress is assumed to consist of two components with the same format as the axial displacement. All other stresses are

zero except for  $r_{xz}$  which must be non-zero in order that prescribed surface displacements may be imposed on the ends of the link. Hence

$$\begin{aligned} r_{xx} &= T_0(x, t) - zT_1(x, t) \\ r_{xz} &= T_2(x, t) \\ r_{yy} &= r_{zz} = r_{yz} = r_{xy} = 0 \end{aligned} \quad (3.12)$$

Similarly, for strains,

$$\begin{aligned} \gamma_{xx} &= S_0(x, t) - zS_1(x, t) \\ \gamma_{xz} &= S_2(x, t) \\ \gamma_{yy} &= \gamma_{zz} = -\nu\gamma_{xx} \\ \gamma_{yz} &= \gamma_{zx} = 0 \end{aligned} \quad (3.13)$$

where the lateral strains are permitted to develop unhindered and  $\nu$  is Poisson's ratio.

Rotatory inertia may be deliberately excluded from the analysis by assuming velocity formats

$$\begin{aligned} p_x &= B(x, t) \\ p_y &= 0 \\ p_z &= C(x, t) \end{aligned} \quad (3.14)$$

The position vector describing the location of the origin of the moving axes  $oxyz$  relative to the inertial frame  $OXYZ$  has components

$$\begin{aligned} r_{ox} &= l_t \cos \theta_4 - L \\ r_{oy} &= 0 \\ r_{oz} &= l_t \sin \theta_4 \end{aligned} \quad (3.15)$$

measured relative to  $o-x-y-z$ , and a general point on the undeformed connecting rod may be defined by

$$r_{Rx} = x, \quad r_{Ry} = y, \quad r_{Rz} = z \quad (3.16)$$

The angular velocity of the rotating frame is

$$\dot{\phi}_x = 0, \quad \dot{\phi}_y = \dot{\theta}_4, \quad \dot{\phi}_z = 0 \quad (3.17)$$

Prescribed deformation displacements are to be imposed on a small region surrounding the centroid of the section at both ends of the link. The flexible link is considered to be pin-pin, and hence

$$\begin{aligned} \text{at } x = 0, \quad \bar{u}_x &= -zw_{,x} \\ \bar{u}_y &= \bar{u}_z = 0 \\ \text{at } x = L, \quad \bar{u}_x &= u_o \\ \bar{u}_y &= \bar{u}_z = 0 \end{aligned} \quad (3.18)$$

Over the remainder of the section at the ends of the link, prescribed surface tractions are imposed. At the rocker-pin end( $x=0$ ) external forces  $P(t)$  and  $Q(t)$  are assumed to be uniformly distributed, so that

$$\text{at } x = 0, \quad \bar{g}_x = \frac{P(t)}{A} \quad (3.19)$$

$$\bar{g}_z = \frac{Q(t)}{A}$$

At the rocker-slider joint, the expressions must incorporate the dynamic effects of the slider on the link and the axial loading again has uniform components. As shown in Fig. 3.3, the slider has normal force  $N(t)$  exerted by the slider guide and a force exerted by the shaker,  $K(t)$

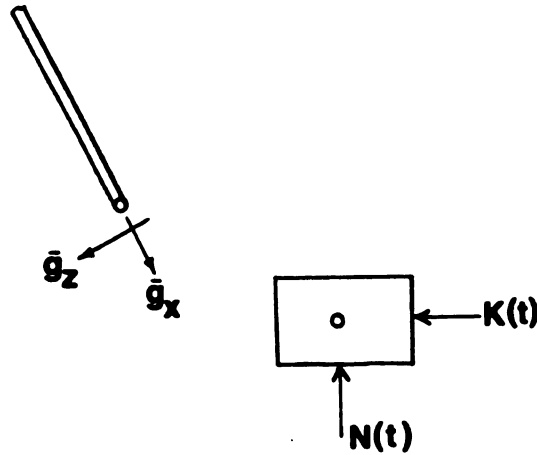


Fig. 3.3 : Forces exerted at the rocker-slider pin joint

The surface tractions are

$$\text{at } x = L, \quad \bar{g}_x = \frac{N(t)}{A} \sin \theta_4 - \frac{K(t)}{A} \cos \theta_4 - \frac{M_s}{A} (\dot{p}_x)_{x=L} \quad (3.20)$$

$$\bar{g}_z = -\frac{N(t)}{A} \cos \theta_4 - \frac{K(t)}{A} \sin \theta_4 - \frac{M_s}{A} (\dot{p}_z)_{x=L}$$

where  $M_s$  is the mass of slider. The flanks of the flexible link are assumed to be unloaded. Hence

$$\bar{g}_x = \bar{g}_y = \bar{g}_z = 0 \quad (3.21)$$

### 3-3 CONSTRUCTION OF THE PROBLEM DEFINITION

The equations of motion and boundary conditions are constructed by substituting the approximating statements (3.11) to (3.21) into the variational eq. (3.10) prior to using the arbitrary independent nature of the variations in the system parameters. Upon substitution into the volume integrals of eq. (3.10) yields

$$\begin{aligned} & \int_x \left\{ - \int_A \rho \delta B [B - (\dot{l}_t \cos \theta_4 - l_t \dot{\theta}_4 \sin \theta_4 + \dot{u}_o - z \dot{w}_{,x} + \dot{\theta}_4 (l_t \sin \theta_4 + z + w))] dA \right. \\ & - \int_A \rho \delta C [C - (\dot{l}_t \sin \theta_4 + l_t \dot{\theta}_4 \cos \theta_4 + \dot{w} - \dot{\theta}_4 (l_t \cos \theta_4 - L + x + u_o - z w_{,x}))] dA \\ & + \int_A [(\delta S_o - z \delta S_1)(T_o - z T_1 - \frac{\partial W}{\partial \gamma_{xx}} + \nu (\frac{\partial W}{\partial \gamma_{yy}} + \frac{\partial W}{\partial \gamma_{zz}})) + \delta S_2 (2T_2 - 4GS_2)] dA \\ & + \int_A (\delta T_o - z \delta T_1) [S_o - z S_1 - \frac{1}{2} ({}^2(u_{o,x} - z w_{,xx}) + w_{,x}^2 + (u_{o,x} - z w_{,xx})^2)] dA \\ & \left. + \int_A \delta T_2 [S_2 - \frac{1}{2} (u_{o,x} - z w_{,xx})(-w_{,x})] dA \right\} \end{aligned}$$

$$\begin{aligned}
& + \int_A (\delta u_o - z \delta w_{,x}) [r_{xj,j} + u_{x,j} k_{kj} + u_{x,k} r_{kj,j} - \rho \dot{p}_x] dA \\
& + \int_A \delta w [r_{zj,j} + u_{z,j} k_{kj} + u_{z,k} r_{kj,j} - \rho \dot{p}_z] dA \Big\} dx = 0 \quad (3.22)
\end{aligned}$$

The first two integrals yield the velocity statements

$$B = \dot{l}_t \cos \theta_4 + \dot{u}_o + w \omega_4 \quad (3.23)$$

$$C = \dot{l}_t \sin \theta_4 + \dot{w} - \omega_4 (x + u_o - L)$$

which may be differentiated to give the absolute accelerations

$$\ddot{B} = \ddot{l}_t \cos \theta_4 + 2\dot{w}\dot{\omega}_4 + w\ddot{\omega}_4 + \ddot{u}_o - \omega_4^2 (x + u_o - L) \quad (3.24)$$

$$\ddot{C} = \ddot{l}_t \sin \theta_4 - 2\dot{u}_o \dot{\omega}_4 + \ddot{w} - w\dot{\omega}_4^2 - \alpha_4 (x + u_o - L)$$

By substituting a strain energy function  $W$  for an isotropic homogenous material into the third integral of expression (3.22), one obtains

$$T_o = ES_o, \quad T_1 = ES_1, \quad T_2 = 2GS_2 \quad (3.25)$$

where  $E$  is the Young's modulus and  $G$  is the modulus of rigidity. The fourth and fifth integrals give

$$\begin{aligned}
S_0 &= u_{0,x} + \frac{1}{2}u_{0,x}^2 + \frac{1}{2}w_{,x}^2 + \frac{I}{2A} w_{,xx}^2 \\
S_1 &= w_{,xx}(1 + u_{0,x}) \\
S_2 &= -\frac{1}{2}u_{0,x} w_{,x}
\end{aligned} \tag{3.26}$$

where  $I$  is the area moment of inertia of the section.

The final pair of integrals in eq. (3.22) must be integrated by parts to give the equations of motion,

$$\begin{aligned}
&\int_V \delta u_0 [\tau_{xx,x} + (u_{x,x} \tau_{xx})_{,x} + (u_{x,z} \tau_{xz})_{,x} - \rho \dot{p}_x] dV \\
&+ \int_V \delta w [(u_{z,x} \tau_{xx})_{,x} - (u_{x,x} \tau_{xz})_{,x} + z \tau_{xx,xx} + (z u_{x,x} \tau_{xx})_{,xx} \\
&+ (z u_{x,z} \tau_{xz})_{,xx} - z \rho \dot{p}_{x,x} - \rho \dot{p}_z] dV = 0
\end{aligned} \tag{3.27}$$

and the natural boundary terms,

$$\begin{aligned}
&\iint_{xy} [(\delta u_0 - y \delta w_{,x}) \tau_{xz} (1 + u_{x,x}) + \delta w \tau_{xz} u_{z,x}]_z dx dy \\
&\iint_{zy} \delta w [\tau_{xz} (1 + u_{x,x}) - z (\tau_{xx,x} + (u_{x,x} \tau_{xx})_{,x} + (u_{x,z} \tau_{xz})_{,x} - \rho \dot{p}_x)]_x dy dz
\end{aligned} \tag{3.28}$$

The final form of equations of motion are constructed by substituting the results (3.24) to (3.26) into eq. (3.27) and performing the integration to give the axial and flexural equations of motion,

$$\begin{aligned}
& EA(u_{o,xx} + u_{o,x}u_{o,xx} + w_{,x}w_{,xx} + \frac{I}{A}w_{,xx}w_{,xxx}) \\
& + (AGu_{o,x}w_{,x}^2)_{,x} + EAu_{o,x}[u_{o,x} + \frac{1}{2}u_{o,x}^2 + \frac{I}{2A}w_{,xx}^2 \\
& + \frac{1}{2}w_{,x}^2 + EIw_{,xx}^2(1 + u_{o,x})]_{,x} - \rho A \dot{B} = 0
\end{aligned} \tag{3.29}$$

$$\begin{aligned}
& EI(w_{,xx}[1 + 2u_{o,x} + \frac{1}{2}u_{o,x}^2 + \frac{1}{2}w_{,x}^2 + \frac{I}{2A}w_{,xx}^2])_{,xx} \\
& - EA(w_{,x}[u_{o,x} + \frac{1}{2}u_{o,x}^2 + \frac{1}{2}w_{,x}^2 + \frac{I}{2A}w_{,xx}^2])_{,x} \\
& - AG(u_{o,x}w_{,x}^2)_{,x} + \rho A \dot{C} = 0
\end{aligned} \tag{3.30}$$

The boundary conditions are derived by combining the last two terms in eq. (3.10) with natural boundary terms (3.28), prior to the substitution of statement (3.18) to (3.21).

At the rocker-pin, prescribed deformations are imposed on a small region at the centroid of the section. On the assumption of plane normal ends to the link, the kinematic boundary conditions at  $x=0$  are

$$u_o = w = 0 \tag{3.31}$$

Over the remainder of the section, the prescribed surface tractions must be combined with the natural boundary terms in expression (3.28) to be evaluated at constant  $x$ . After permitting independent variations in the parameters, integration over the beam section yields the following statements at,



at  $x = 0$ ,

$$\begin{aligned}
 P(t) + EA[u_{o,x} + \frac{1}{2}u_{o,x}^2 + \frac{1}{2}w_{,x}^2 + \frac{I}{2A}w_{,xx}^2](1 + u_{o,x}) \\
 + EIw_{,xx}^2(1 + u_{o,x}) + AGu_{o,x}w_{,x}^2 = 0
 \end{aligned} \tag{3.32a}$$

$$EIw_{,xx}[1 + 3u_{o,x} + \frac{3}{2}u_{o,x}^2 + \frac{1}{2}w_{,x}^2 + \frac{I}{2A}w_{,xx}^2] = 0 \tag{3.32b}$$

$$\begin{aligned}
 Q(t) + EAw_{,x}(u_{o,x} + \frac{1}{2}u_{o,x}^2 + \frac{1}{2}w_{,x}^2 + \frac{I}{2A}w_{,xx}^2) \\
 - EI(w_{,xxx}[1 + u_{o,x}] - w_{,xx}[w_{,xxx} - u_{o,xx}]) (1 + u_{o,x}) + AGu_{o,x}^2w_{,x} \\
 - EI(w_{,xx}[u_{o,x} + \frac{1}{2}u_{o,x}^2 + \frac{1}{2}w_{,x}^2 + \frac{I}{2A}w_{,xx}^2])_{,x} = 0
 \end{aligned} \tag{3.32c}$$

These equations simply complete the problem-definition, since the values of the pin forces  $P$  and  $Q$  cannot be determined until the problem has been solved for the deformation displacements.

On the beam flanks, the prescribed surface traction condition must be combined with the natural boundary terms in eq. (3.28) to be evaluated at constant  $y$ . The result is identically zero.

The statement for the prescribed surface tractions which are imposed on the major portion of the beam section at the rocker-slider pin must be combined with the natural boundary term and this yields, upon integration,

at  $x = L$ ,

$$\begin{aligned}
& N(t)\sin\theta_4 - K(t)\cos\theta_4 - M_s(\dot{p}_x)_{x=L} - EIw_{,xx}^2(1 + u_{o,x}) - AGu_{o,x}w_{,x}^2 \\
& - EA(1 + u_{o,x})(u_{o,x} + \frac{1}{2}u_{o,x}^2 + \frac{1}{2}w_{,x}^2 + \frac{I}{2A}w_{,xx}^2) = 0 \quad (3.33a)
\end{aligned}$$

$$EIw_{,xx}[1 + 3u_{o,x} + \frac{3}{2}u_{o,x}^2 + \frac{1}{2}w_{,x}^2 + \frac{I}{2A}w_{,xx}^2] = 0 \quad (3.33b)$$

$$\begin{aligned}
& - N(t)\cos\theta_4 - K(t)\sin\theta_4 - M_s(\dot{p}_z)_{x=L} \\
& - EAw_{,x}(u_{o,x} + \frac{1}{2}u_{o,x}^2 + \frac{1}{2}w_{,x}^2 + \frac{I}{2A}w_{,xx}^2) \\
& + EI(w_{,xx}[1 + u_{o,x}] - w_{,xx}[w_{,xxx} - u_{o,xx}])(1 + u_{o,x}) \\
& + EI(w_{,xx}[u_{o,x} + \frac{1}{2}u_{o,x}^2 + \frac{1}{2}w_{,x}^2 + \frac{I}{2A}w_{,xx}^2])_{,x} = 0 \quad (3.33c)
\end{aligned}$$

### 3-4 AN APPROXIMATE SOLUTION

The problem definition is now complete since equations of motion and the corresponding boundary conditions have been constructed. Thus the objective is to simplify the equations sufficiently to permit the use of standard solution procedures.

The forcing frequency of the rocker link is much lower than the first natural frequency in the axial mode, and hence the axial vibrations may be neglected [23]. If second and higher-order terms are assumed to be small in eq. (3.29) and (3.33a), then the integration of eq. (3.29) with respect to  $x$  gives a general statement for the axial force in the link:

$$\begin{aligned}
 EAu_{o,x} - \rho A \ddot{l}_t \cos \theta_4 (x - L) - \rho A \omega_4^2 \left[ \frac{1}{2} x^2 - Lx + L^2 \right] \\
 + N(t) \sin \theta_4 - K(t) \cos \theta_4 - M_s (\dot{p}_x)_{x=L}
 \end{aligned} \quad (3.34)$$

Attention is now focused on eq. (3.30) which governs the flexural vibrations of the link. Upon neglecting the shear term, second and higher-order terms in the coefficient of EI and third-order terms in the coefficient of EA, this equation reduces to

$$EIw_{,xxxx} - EAu_{o,x} w_{,xx} - EAu_{o,xx} w_{,x} + \rho A \ddot{C} = 0 \quad (3.35)$$

The axial force statement (3.34) may be substituted into eq. (3.35) to give

$$\begin{aligned}
 EIw_{,xxxx} - [\rho A x \ddot{l}_t \cos \theta_4 - \rho A \omega_4^2 \left( \frac{1}{2} x^2 - Lx \right) + N \sin \theta_4 - K \cos \theta_4 - M_s (\dot{p}_x)_{x=L} \\
 - m \ddot{l}_t \cos \theta_4 - \frac{1}{2} m L \omega_4^2] w_{,xx} + [-\rho A \ddot{l}_t \cos \theta_4 + \rho A \omega_4^2 (x-L)] w_{,x} \\
 + \rho A [\ddot{l}_t \sin \theta_4 + \ddot{w} - \omega_4^2 - \alpha_4 (x-L)] = 0
 \end{aligned} \quad (3.36)$$

where  $m(m=\rho AL)$  is the mass of the flexible link

A solution procedure in which normal modes are used will be adopted for this non-linear differential equation. Since any deflection of the beam may be expressed as the sum of deflections in the various principal modes [24], the standard solution can be written as

$$w(x, t) = \sum_{n=1}^n W_n(t) \phi_n(x) \quad (3.37)$$

where  $W_n(t)$  are unknowns and  $\phi_n(x)$  are the mode shapes. In accordance with the standard approach, the derivatives of eq. (3.37) are substituted into eq. (3.36) and the orthogonality condition utilized by multiplying the resulting equation by  $\phi_m(x)$  before integrating each term over the length of the rocker link. This gives an equation of the form

$$\begin{aligned} \ddot{W}(t) + W(t) & \left[ \frac{EIc_1}{\rho Ac_7} - \frac{c_2 + c_5}{c_7} L \omega_4^2 + \frac{c_3 + 1/2c_6 - c_7}{c_7} \omega_4^2 + \frac{c_4}{\rho Ac_7} (K \cos \theta_4 \right. \\ & \left. - N \sin \theta_4 + \frac{1}{2} m L \omega_4^2) + \left( \frac{c_4}{c_7} L - \frac{c_2 + c_5}{c_7} + \frac{M_s c_4}{\rho A c_7} \right) \ddot{\theta}_t \cos \theta_4 \right] \\ & - \left( \frac{c_9 - c_8 L}{c_7} \right) \alpha_4 - \frac{c_8}{c_7} \ddot{\theta}_t \sin \theta_4 \end{aligned} \quad (3.38)$$

where the constants  $c_i$  ( $i = 1, 2, \dots, 9$ ) are given by

$$\begin{aligned} c_1 &= \int_0^L \phi_n \phi_{n,xxxx} dx & c_2 &= \int_0^L \phi_n \phi_{n,x} dx \\ c_3 &= \int_0^L \phi_n \phi_{n,x} x dx & c_4 &= \int_0^L \phi_n \phi_{n,xx} dx \\ c_5 &= \int_0^L \phi_n \phi_{n,xx} x dx & c_6 &= \int_0^L \phi_n \phi_{n,xx} x^2 dx \\ c_7 &= \int_0^L \phi_n^2 dx & c_8 &= \int_0^L \phi_n dx \end{aligned} \quad (3.39)$$

$$c_0 = \int_0^L \phi_n x dx$$

Equation (3.38) is an inhomogeneous Hill's equation and the first term in the coefficient of  $W$  yields the natural frequency of the stationary link. If  $\omega_n$  denotes the natural frequency of the link, eq. (3.38) can be written in simpler form as

$$\ddot{W}(t) + W(t)[\omega_n^2 + r(t)] = R(t) \quad (3.40)$$

For the pinned-pinned beam the form of the principal modes are sine curves [24]. Hence the characteristic function is

$$\phi_n(x) = \sin \frac{n\pi x}{L} \quad (3.41)$$

while the value of the  $n^{\text{th}}$  principal co-ordinate  $W_n$  as that which gives unit amplitude to the sine wave. Upon substitution of eq. (3.41) into eq. (3.39) and integrating them, the  $c_i$  values may be found directly. Since the transverse deflection at the midspan of the rocker link is of interest, the mode shape  $\phi_n(x)$  appearing in (3.37) may be evaluated at  $x = L/2$ , hence

$$\phi_n(x = L/2) = \sin \frac{n\pi}{2} \quad (3.42)$$

The next step is to solve the Hill's eq. (3.38) for the time dependent amplitude  $W(t)$  by a viable method. The midspan deflection of the link may then be evaluated from (3.37) by summing over the desired number of terms.

## CHAPTER 4

### SOLUTION TO HILL'S EQUATION

The Hill's equation (3.38) obtained in the preceding chapter is linear inhomogeneous differential equation with periodic coefficients and the system is subjected to forcing excitations of periodic nature. This equation can be solved for both elastodynamic and quasi-static responses, since the kinematic characteristics of the intelligent mechanism are known. Only the steady-state solution is considered here, which implies the system is stable and this will be verified in chapter 6. The steady-state response would the amplitude of deflection of the rocker link.

#### 4-1 QUASI-STATIC RESPONSE

A straight-forward method of solving the Hill's equation is to neglect the dynamic term( $\ddot{W}$ ) and obtaining the solution directly, which is termed as quasi-static solution. Upon neglecting the dynamic term, the Hill's equation becomes

$$W(t)[\omega_n^2 + r(t)] = R(t) \quad (4.1)$$

Hence the amplitude of deflection may be evaluated on a digital computer from the equation

$$W(t) = \frac{R(t)}{[\omega_n^2 + r(t)]} \quad (4.2)$$

## 4-2 ELASTODYNAMIC RESPONSE

The steady-state solution to Hill's equation is termed as elastodynamic response. An explicit expression for the steady-state periodic response is possible, but for the system under investigation an analytical determination is not feasible. A straightforward numerical procedure developed by Hsu [18] is used here.

### 4-2.1 MATRIX NOTATIONS

The Hill's equation under periodic forcing can be written in standard state-variable form as

$$\dot{\mathbf{x}}(t) = \mathbf{C}(t)\mathbf{x}(t) + \mathbf{f}(t) \quad (4.3)$$

where

$$\mathbf{x}(t) = \begin{Bmatrix} x_1(t) \\ x_2(t) \end{Bmatrix} = \begin{Bmatrix} W(t) \\ \dot{W}(t) \end{Bmatrix}, \quad \mathbf{C}(t) = \begin{bmatrix} 0 & 1 \\ -[\omega_n^2 + r(t)] & 0 \end{bmatrix},$$

$$\mathbf{f}(t) = \begin{Bmatrix} 0 \\ R(t) \end{Bmatrix}$$

In the above equation  $\mathbf{x}$  is a vector,  $\mathbf{C}$  is real coefficient matrix periodic in  $t$  with period  $\tau_0$  and  $\mathbf{f}$  a vector also periodic in  $t$  but with period  $\tau_f$ . For the intelligent mechanism,  $\tau_0$  would be the period of crank rotation and  $\tau_f$  as the period of shaker excitation.



## 4-2.2 NUMERICAL PROCEDURE

Let  $\Phi(t)$  with  $\Phi(0) = I$  be the fundamental matrix for the solution of the homogeneous equation (assuming  $f(t)=0$ ) corresponding to (4.3). Then the solution of (4.3) is given by

$$\mathbf{x}(t) = \Phi(t)\{\mathbf{x}(0) - (I - H)^{-1}Hg\} + \mathbf{x}_f(t), \quad (4.4)$$

where the first term is the solution to homogeneous equation and  $\mathbf{x}_f(t)$  is steady-state response and is given by

$$\mathbf{x}_f(t) = \Phi(t)\left\{\int_0^t \Phi^{-1}(s)f(s)ds + (I - H)^{-1}Hg\right\} \quad (4.5)$$

The quantities  $\int_0^t \Phi^{-1}(s)f(s)ds$  and  $g$  appearing in (4.5) are

evaluated by simply using the Trapezoidal rule of numerical integration. In this manner from Hsu, the final form of steady-state solution is given by

$$\mathbf{x}_f(t_\kappa) = \mathbf{x}_\kappa + \Phi(t_\kappa)(I - H)^{-1}\mathbf{x}_K, \quad \kappa = 0, 1, 2, \dots, K \quad (4.6)$$

where

$$\mathbf{x}_0 = 0$$

$$x_{\kappa} = \Delta \left\{ \frac{1}{2} \begin{bmatrix} \kappa \\ \Pi \\ j-1 \end{bmatrix} \varphi_j(\Delta) \right\} f_0 + \sum_{i=2}^{\kappa} \begin{bmatrix} \kappa \\ \Pi \\ i-2 \end{bmatrix} \varphi_i(\Delta) f_{i-1} + \frac{1}{2} f_{\kappa} \quad (4.7)$$

and

$$H = \begin{bmatrix} K \\ \Pi \\ j-1 \end{bmatrix} \varphi_j(\Delta) \quad (4.8)$$

$\Phi(0) = I$ , identity matrix

$$\Phi(t_{\kappa}) = \begin{bmatrix} \kappa \\ \Pi \\ j-1 \end{bmatrix} \varphi_j(\Delta), \quad \kappa = 1, 2, \dots, K \quad (4.9)$$

$$f_j = f(t_j) \quad (4.10)$$

The time step  $\Delta$  is obtained by dividing the crank period  $\tau_0$  by a large positive integer  $K$ , i.e.

$$\Delta = \frac{\tau_0}{K} \quad (4.11)$$

Note that the equations are written by assuming similar frequencies for the crank and shaker excitation.

To evaluate numerically the periodic steady-state response,  $x_f(t)$  will be evaluated at the discrete station points  $t = t_{\kappa}$ , where

$$t_{\kappa} = \kappa \Delta, \quad \kappa = 0, 1, 2, \dots, K \quad (4.12)$$

An efficient expression for  $\varphi_j(\Delta)$  appearing in the above equations may be evaluated using Scheme I of Hsu [18], and it is given by

$$\varphi_j(\Delta) \approx \exp(C_j \Delta) \quad (4.13)$$

By using the coefficient matrix  $C$  and the methodology found in reference [25], eq. (4.13) can be written as

$$\varphi_j(\Delta) = e^{-\Delta} \begin{bmatrix} \cos \omega_j \Delta & \frac{1}{\omega_j} \sin \omega_j \Delta \\ -\omega_j \sin \omega_j \Delta & \cos \omega_j \Delta \end{bmatrix} \quad (4.14)$$

where  $\omega_j = [\omega_n^2 + r_j(t)]^{1/2}$

Upon substituting equations (4.7) to (4.12) and (4.14) into eq. (4.6), the steady-state response or the amplitude of deflection of the rocker link may be evaluated at discrete time step.

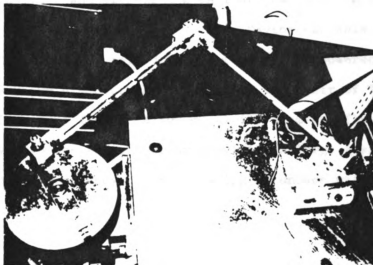
## **CHAPTER 5**

### **EXPERIMENTAL INVESTIGATION**

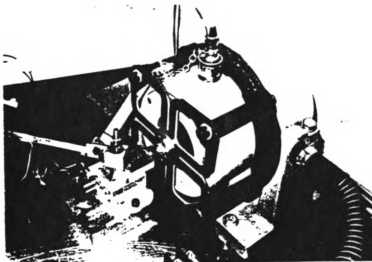
#### **5-1 EXPERIMENTAL APPARATUS**

A photograph of the experimental intelligent mechanism is presented in Fig. 5.1. The rigid coupler link is manufactured from aluminum and the flexible rocker link is from steel. At the end of each link, two clearance holes were drilled. These holes accommodated socket screws which clamped each specimen to the bearing housing. Identical ball bearings of type R4 DB 12 instrument ball bearings supplied by FAG Bearing Limited were used at crank-ground pin and at rocker-slider end. The rocker pin was mounted on R3Z ball bearing and a cleavage design joint was used for coupler-rocker end as shown at the top of Fig. 5.1. Each bearing housing in the mechanism was preloaded using a Dresser Industries torque limiting screw driver calibrated to  $\pm 1$  in-lbf to eliminate radial clearance, otherwise the impact loading associated with bearing clearances would cause the links to have larger deflections.

One end of the rocker link was connected to a Microslides Inc. 2020 cross-roller slide assembly which permitted translational motion as shown in Fig. 5.2. This precision assembly was then bolted to a force transducer, which permitted the force exerted by the shaker on the slider to be carefully monitored. An accelerometer was mounted on the slide assembly parallel to the translational motion to measure the kinematic characteristics imposed by the vibrator, as shown in Fig. 5.2.



**Fig. 5.1 : Experimental Intelligent Mechanism**



**Fig. 5.2 : Electrodynamic Shaker-Slider Assembly**

The mechanism was bolted to a large cast-iron test stand which was bolted to the floor and also to the wall of the laboratory to provide a substantial rigid foundation. A 0.75 h.p. Dayton variable speed d.c. electric motor which was bolted to the test stand, powered the linkage through a 19.05 mm diameter shaft supported on a pair of Timken tapered roller bearings type TS4A-6. A 100 mm (4 in) diameter flywheel (see Fig. 5.1) was keyed to the shaft thereby providing a large inertia to ensure a constant crank frequency, when operating in unison with the motor's speed controller.

The data for the mechanism is shown in Table 5.1. The initial ground link length was 381 mm and upon the shaker excitation, it is variable with time. The net mass of the flexible link was 22.6 grams. This data will be used for computer simulation in the following chapters.

	Crank (rigid)	Coupler (rigid)	Rocker (flexible)
Link length, pin to pin (mm)	50	305	293.6
Mass, gm (including bearings and joints)	*	157	146.7
Depth, mm (in the plane perpen. to the mechanism)	*	19.43	10.2
Width, mm (in the plane of mechanism)	*	6.25	0.838
$r_i$ , meters (center of mass, see Fig. 2.3)	0.0	0.176	0.192
Mass moment of inertia, $\text{Kg-m}^2$ (see Fig. 2.3)	*	0.005286	0.00722

Modulus of elasticity for rocker link,  $E=207 \text{ Gpa}$   
 Mass density of rocker link,  $\rho = 9294.3 \text{ Kg/m}^3$

Area moment of inertia,  $I=3.9588 \times 10^{-13} \text{ m}^4$

Mass of slide assembly,  $M_s = 0.415 \text{ Kg}$

\* Flywheel was used to provide large inertia to insure  
 a constant crank frequency

Table 5.1 : Data for Intelligent Mechanism

## 5-2 INSTRUMENTATION

A schematic diagram of the instrumentation employed in the experimental investigation is shown in Fig. 5.3. The rated speed of the electric motor was measured in revolutions per minute(rpm) by a Hewlett Packard 5314A Universal Counter which was activated by an electro-magnetic pickup model 58423, manufactured by Electro Corp., sensing a sixty tooth spur gear mounted on the drive shaft of the rig. The gear is shown in Fig. 5.4. The arrangement provided visual feedback to the operator by adjusting the speed controller of the motor in order achieve the desired crank speed.

The experimental result presents the variation of link deflections with crank angle. Strain gages were bonded to the midspan of the rocker link and the midspan deflections were monitored by a Micromasurements Group Inc., strain gage conditioner/amplifier system type 2100. In order to relate the strain gage signal to the configuration of the experimental mechanism, another transducer arrangement was established. An Airpax type 14-0001 zero velocity digital pickup was employed to sense the bolt-head at the end of the crank, when the mechanism is in the position of zero-degree crank angle. This long hexagonal transducer is shown in Fig. 5.4

In order to excite the shaker simultaneously with crank motion, the signal from Airpax pickup at zero-degree crank angle configuration will be fed to wave generator. A Wavetek digital arbitrary function generator permits arbitrary waveforms to be generated for a wide range of frequencies. A desired wave function is programmed into the Wavetek



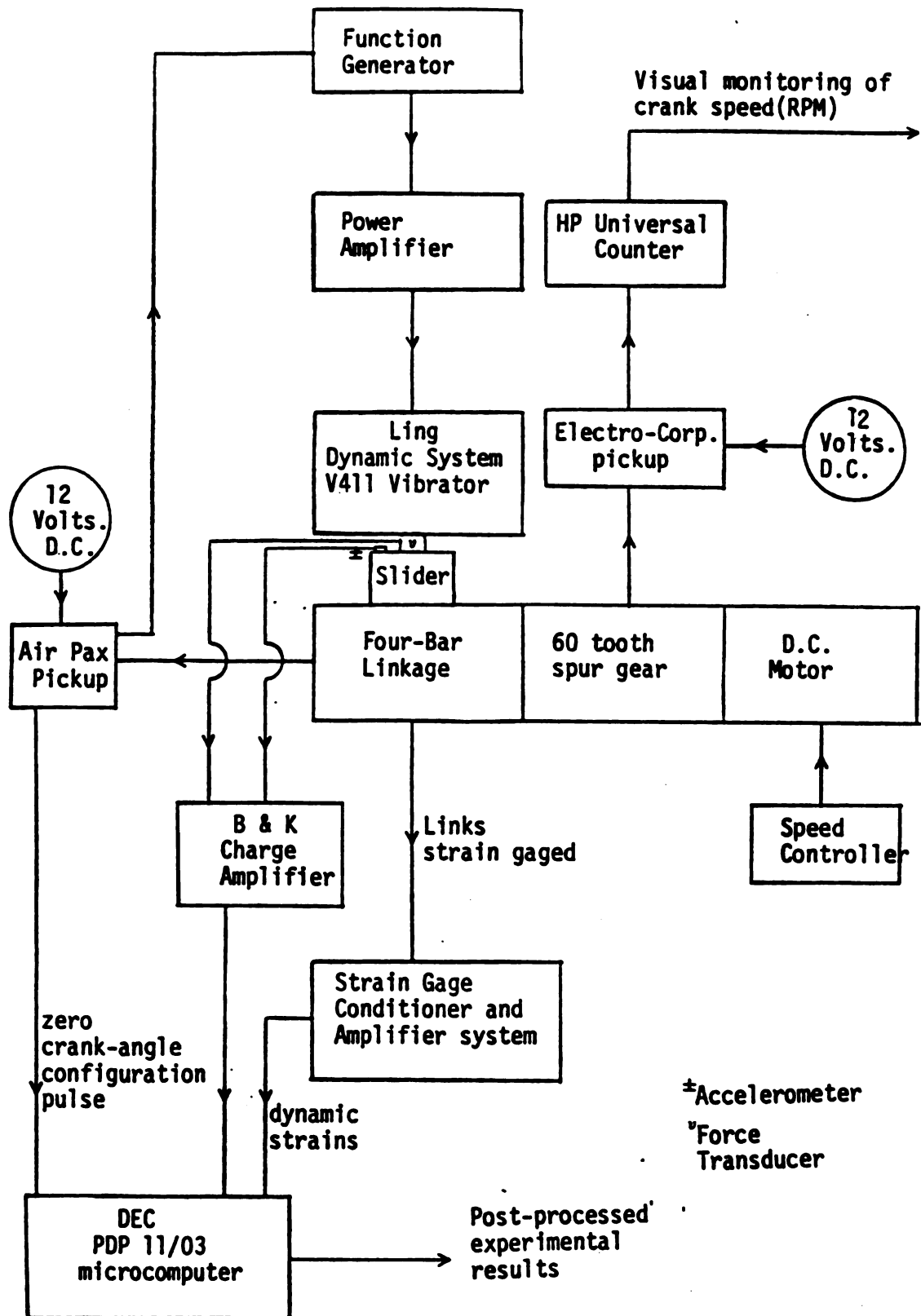


Fig. 5.3 : Schematic Diagram of the Instrumentation

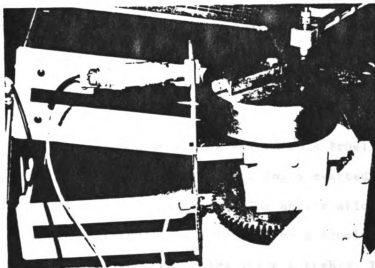


Fig. 5.4 : Assembly of Crank and Airpax Pickup

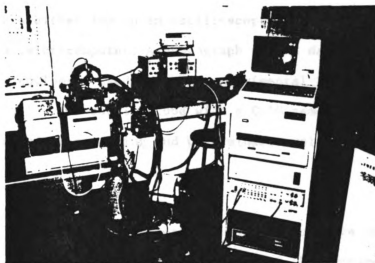


Fig. 5.5 : Data-Acquisition System and Equipment

and the signal is amplified by Hafler power amplifier model P500, prior to feeding it to the shaker. The shaker is an air-cooled Ling Dynamic Systems type V411 vibrator, which upon converting electrical current into mechanical force will permit translational motion to the slide-assembly.

The precision assembly which was bolted to a Bruel & Kjaer force transducer, type 8200, which permitted the force exerted by the shaker on the slider to be carefully monitored. The acceleration imposed by the shaker upon the slide-assembly was monitored by a Bruel & Kjaer accelerometer type 4731, mounted on the slide-assembly. The output from the two transducers were fed to a Bruel & Kjaer charge amplifier type 2635, which enabled the force and displacement, velocity and acceleration characteristics of the slide-assembly to be monitored.

The mechanism configuration signal, the output from the gages and transducers were either fed to an oscilloscope or to a Digital Equipment Corp. PDP 11/03 microcomputer. A photograph of the data-acquisition system and the equipment used for this experimental investigation is shown in Fig. 5.5. The oscilloscope with a C-5C camera attachment was used for photographic recording and preliminary evaluation of the response data.

The BNC cables from the experimental apparatus were connected to an input-output module, bolted to the cabinet of the computer. This device had 16 analog-digital channels, 4 digital-analog channels and two schmidt triggers. Using the code developed for digital data-acquisition, the kinematic output and flexural response signal was recorded from the

zero crank angle position through 360 degrees by firing one of the Schmidt triggers.

### 5-3 EXPERIMENTAL PROCEDURE

The experimental procedure involved first determining the natural frequency of the stationary rocker link, so that the mechanism can be operated away from the undesirable vibrations. The mechanism under stationary condition, the rocker link was deflected and released and the transient vibration was recorded on the oscilloscope prior to photographically recording it on the camera. The result is presented in Fig. 5.6. The mechanism was then operated at constant crank frequency by locking the cross-roller slide assembly in order to create a classical four-bar linkage. The preliminary experimental work was to obtain a frequency-response curve, so that desirable operating speed could be chosen.

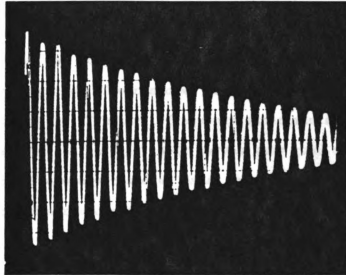


Fig. 5.6 : Transient Response of Rocker Link ( $\omega_n = 18.75$  Hz)

The frequency response of the flexible rocker link is investigated for a wide range of operating speeds. The theoretical elastodynamic response is obtained by solving the Hill's equation. The experimental results were obtained by operating the four-bar linkage through a range of crank speeds and recording the resulting midspan amplitude of the rocker link. The theoretical natural frequency of the rocker link was computed from the Hill's eq. and it is compared with experimentally obtained result below,

$$\begin{aligned}\omega_{n,th} &= 19.32 \text{ Hz (1159 rpm)} \\ \omega_{n,ex} &= 18.75 \text{ Hz (1125 rpm)}\end{aligned}\tag{5.1}$$

Since the Hill's equation does not incorporate damping, the theoretical natural frequency was found to be slightly higher than the experimental result.

Fig. 5.7 shows the frequency response curve from analytical and experimental investigation. The response regime shows the resonance condition when the ratio of natural frequency(experimental result) to operating frequency is an integer. Both curves show good correlation. Having defined the frequency response data, operating speeds can be chosen remote from the resonance condition.

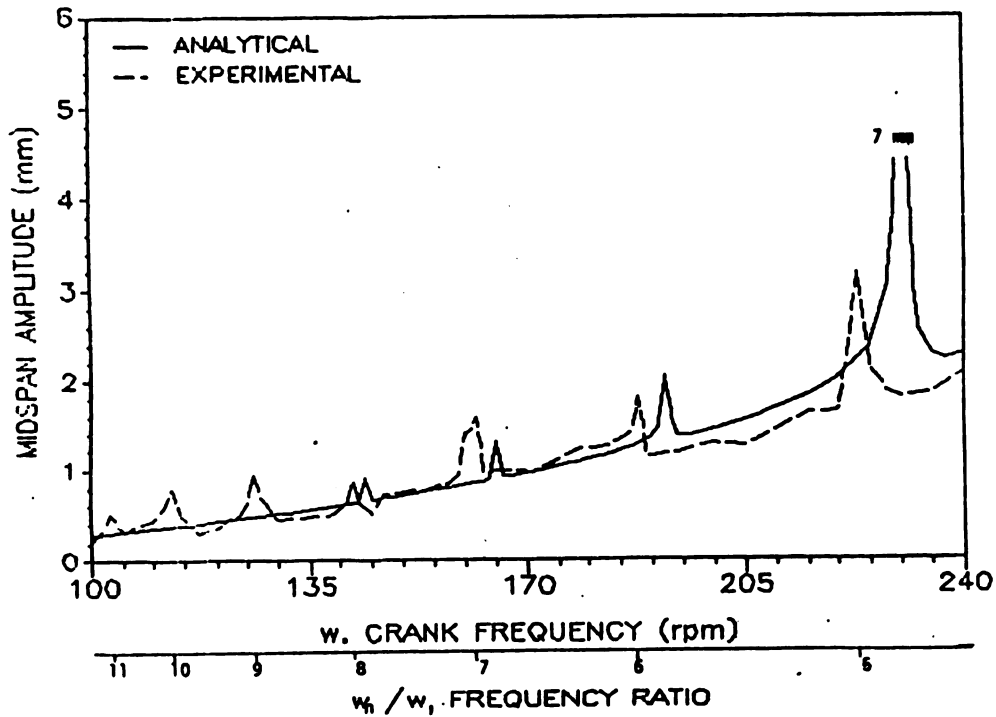


Fig. 5.7 : Frequency-response curves for the four-bar linkage

The classical four-bar linkage was then operated at the chosen speed to obtain the transverse deflection curves upon which the response curves with the shaker excited will be compared. The data was then digitally filtered with low-bound frequency set at approximately 30 Hz and 100 Hz to yield quasi-static and elastodynamic response respectively. The digital filtering also removed electromagnetic and other noise sources which may have occurred during the course of the experiment.

In order to excite the shaker, the prismatic joint was unlocked prior to programming a waveform into the function generator. The displacement of the slider was carefully monitored by controlling the amplifier gain. Upon maintaining a constant crank speed, the mechanism was operated for at least two minutes in order to allow the link

deflections to settle down to a periodic nature. This was visually monitored on the oscilloscope along with the displacement, velocity and acceleration of the slider.

Experimental results were obtained by implementing the following procedure. The signal from the strain gage instrumentation was fed to the PDP microcomputer and the results were digitally filtered. The data was then post-processed by multiplying the digitized response by a strain-deflection calibration factor for the rocker link specimen. This factor was obtained by supporting the link at the ends on knife edges in a calibration fixture shown in Fig. 5.8, prior to subjecting the midspan to a series of known monotonically increasing transverse deflections which were imposed and measured by a micrometer attachment on the fixture. The corresponding voltages from the strain gages bonded to the link were also recorded to relate strain magnitude to midspan deflection.

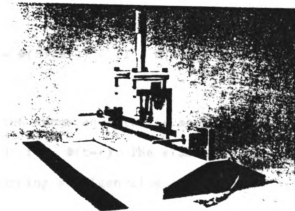


Fig. 5.8 : Link Calibration-Fixation



## CHAPTER 6

### STABILITY ANALYSIS

#### 6-1 STABILITY OF MOTION

It is well known that for systems with time-periodic coefficients which are free from external forcing, the behavior of the system can be investigated according to Floquet theory [26]. When the system is subjected to periodic-forcing and when the homogeneous equation is stable or asymptotically stable, then a key result one will be interested in is the steady-state response of the system under that forcing. Hence, the stability of the mechanism is investigated by means of Hill's homogeneous equation.

The Hill's homogeneous equation is given by

$$\ddot{W}(t) + W(t)[\omega_n^2 + r(t)] = 0 \quad (6.1)$$

and the corresponding solution to (6.2) is reproduced from eq. (4.4) of chapter 4,

$$\mathbf{x}_h(t) = \Phi(t)(\mathbf{x}(0) - (\mathbf{I} - \mathbf{H})^{-1}\mathbf{H}\mathbf{g}) \quad (4.4)$$

It is argued that the above equation is stable only if  $\Phi(t)$  is stable at the system's period, i.e.  $\Phi(t-\tau)$ . The stability of this matrix is determined by performing an eigenvalue analysis.

The general procedure for eigenvalue analysis is as follows:

1) Compute eigenvalues of  $\Phi(r)$

let  $\lambda_1, \dots, \lambda_n$  be the eigenvalues

2) Choose  $\lambda_n = 1$ , one eigenvalue will always be equal to 1

3) The remainder must lie inside of the unit circle in the complex plane for stability.

i.e. system is stable if  $|\lambda_i| < 1 \quad i=1, \dots, n-1$

system is unstable if  $|\lambda_i| > 1 \quad \text{for all } i$

Fig. 6.1 shows the analytically obtained frequency response curves for the four-bar linkage and intelligent mechanism, where stability analysis has been performed for a wide range of operating speeds. The shaker displacement for the modified linkage was chosen in the range 0 to -1.35 mm (The viable waveform will be varified in chapter 7). The discontinuos portion of the curves are parts where the steady-state response has no meaning because the homogeneous system is unstable. Note that the instability occurs at the same region for both mechanisms. In the following chapters, steady-state solution is utilized by operating in the stable region.

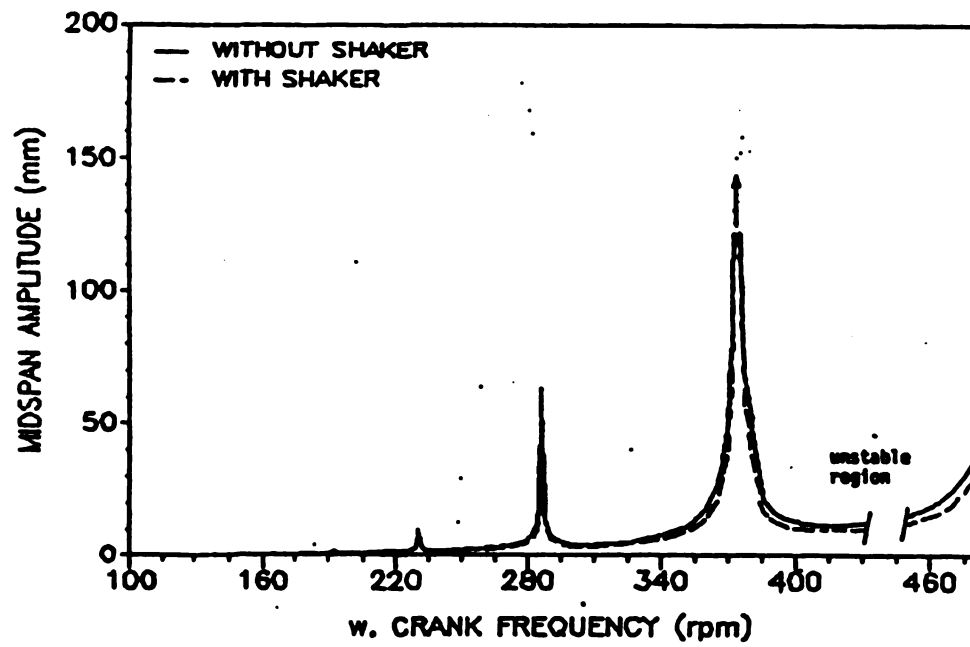


Fig. 6.2 : Analytical Frequency-response curves

## CHAPTER 7

### ELASTODYNAMIC RESPONSE OF THE UNMODIFIED LINKAGE AND THE SYNTHESIS OF THE SHAKER/SLIDER MOTION

#### 7-1 RESPONSE CURVES FOR THE FLEXIBLE FOUR-BAR LINKAGE

The first set of results of interest is the midspan transverse deflection of the flexible link of a classical four-bar linkage. The analytical result is the steady-state solution obtained numerically from eq. (4.6) by setting the shaker input to zero (i.e.  $\ddot{y}_t=0$ ). These analytical results are then compared with experimentally obtained elastodynamic deflection in order to verify the correlation between them. A good correlation of these results will allow to make better prediction of the response with the shaker in motion.

The main assumptions made in formulating the computer model for simulations are:

- (1) All bearings were considered frictionless and without clearance.
- (2) The crank speed was assumed constant.
- (3) The kinematic analysis of the flexible link was based on the assumption that it was a rigid body
- (4) Damping was neglected in the derivation of the equations of motion.

Figures 7.1, 7.2, 7.3 and 7.4 presents a comparison of the elastodynamic response of the rocker link from analytical and experimental investigations at crank frequencies of 148, 170, 200 and 215 rpm respectively. These curves comprises two components: the quasi-

static response at the mechanism's operating frequency and a high-frequency component at approximately the link's fundamental natural frequency in flexure. The quasi-static response of the rocker link obtained at 200 rpm is compared in Fig. 7.5

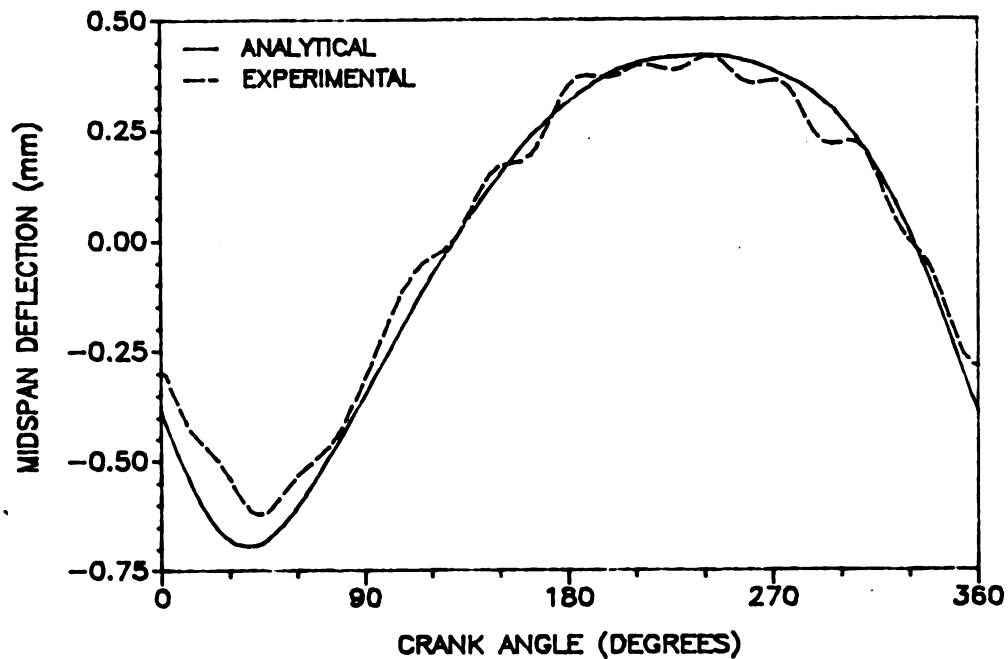


Fig. 7.1 : Elastodynamic Response of the Four-bar  
Linkage at 148 rpm

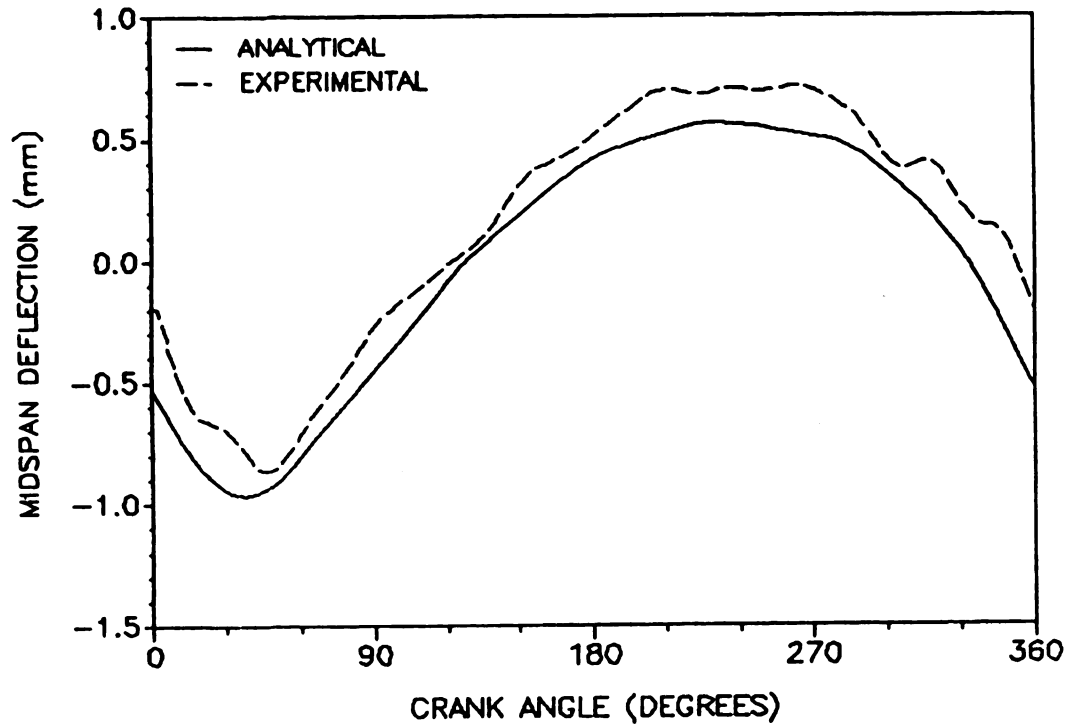


Fig. 7.2 : Elastodynamic Response of the Four-bar  
Linkage at 170 rpm

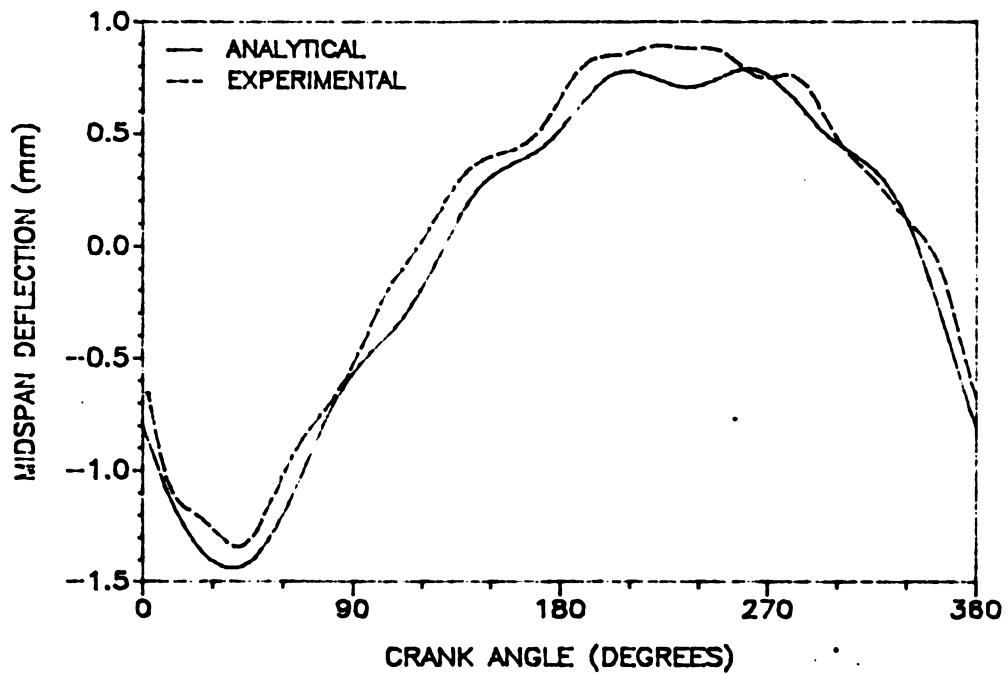


Fig. 7.3 : Elastodynamic Response of the Four-bar  
Linkage at 200 rpm

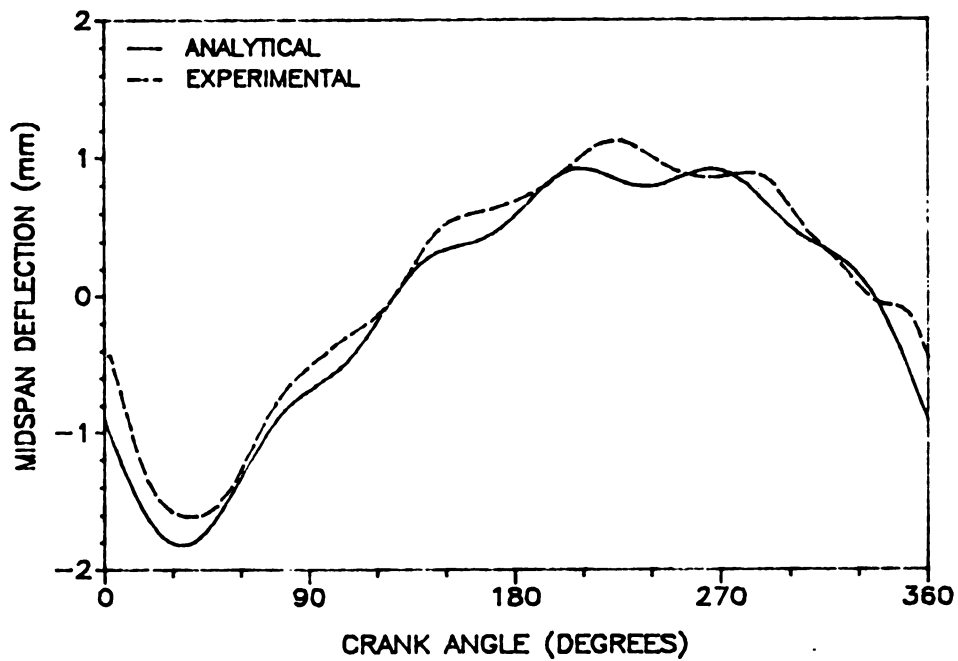


Fig. 7.4 : Elastodynamic Response of the Four-bar linkage at 215 rpm

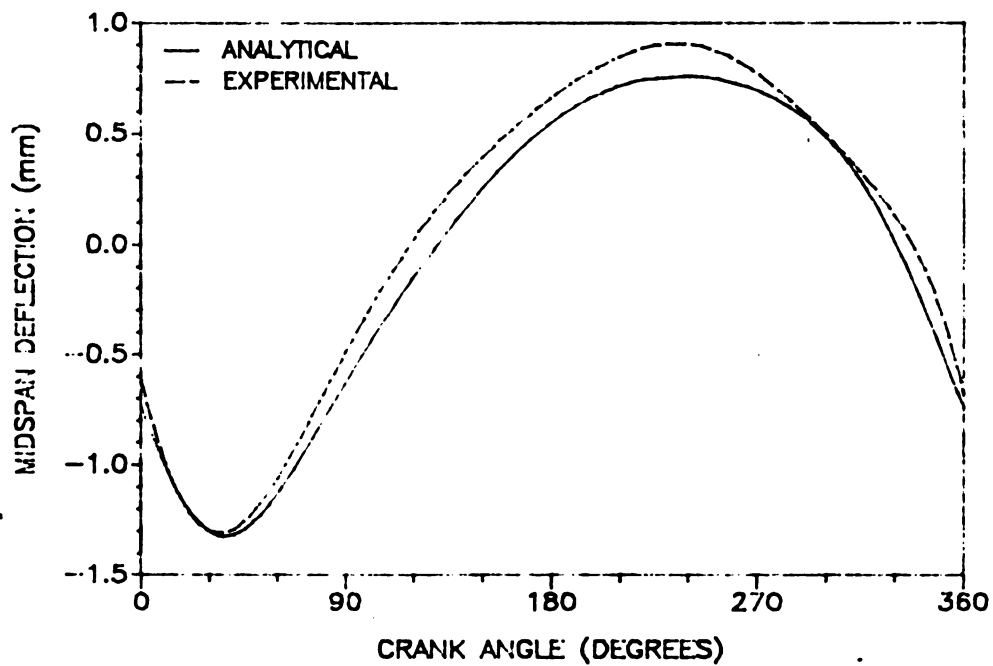


Fig. 7.5 : Quasi-static Response of the Four-bar Linkage at 200 rpm

## 7-2 CURVE SYNTHESIS FOR SHAKER/SLIDER MOTION

### 7-2.1 JUSTIFICATION OF WAVEFORM

The current mode of operation of the four-bar linkage may not satisfy the prescribed design specification; namely the amplitude of deflection may be greater than a prescribed quantity. Under these circumstances, a linkage with two-degrees of freedom may provide a solution whereby the motion of the slider would be controlled in a prescribed manner in order to reduce the deflections of the rocker link. This philosophy requires the ability to synthesize a suitable waveform for the shaker/slider motion.

A general waveform of sine function is considered here.

$$l_t = A_s \sin(\omega_s t + \phi_s), \quad (7.1)$$

where  $A_s$  is the amplitude of slider motion,  $\omega_s$  is the frequency of excitation and  $\phi_s$  is the phase between crank motion and shaker excitation. Hence, there are 3 independent variables that need to be evaluated such that when eq. (7.1) is substituted into the Hill's eq. (3.38), the amplitude of deflection is reduced in comparison to classical four-bar linkage (i.e.  $\ddot{l}_t = 0$ ). The proposed waveform becomes more complicated if  $l_t$  is assumed to be function of sine and cosine terms. A less cumbersome methodology is to excite the shaker using a waveform based on the profile of the link response. This waveform



requires a theoretical justification to insure the vibrational response does not exceed the prescribed quantity.

For the purpose of discussion, the Hill's equation (3.38) is reproduced here. The methodology proposed herein focuses on the right-hand-side of the equation; namely the kinematic variables which provide the principal system excitation in a high-speed mode of operation. Since the shaker inertial term ( $\ddot{l}_t$ ) appears on both sides of the equation, reducing the angular acceleration of the rocker link ( $\alpha_4$ ) by means of shaker excitation does not guarantee a reduction in the elastodynamic response.

$$\begin{aligned} \ddot{W}(t) + W(t) & \left[ \frac{EIc_1}{\rho Ac_7} - \frac{c_2 + c_5}{c_7} L \omega_4^2 + \frac{c_3 + 1/2c_6 - c_7}{c_7} \omega_4^2 + \frac{c_4}{\rho Ac_7} (K \cos \theta_4 \right. \\ & \left. - N \sin \theta_4 + \frac{1}{2} m L \omega_4^2) + \left( \frac{c_4}{c_7} L - \frac{c_2 + c_5}{c_7} + \frac{M_s c_4}{\rho Ac_7} \right) \ddot{l}_t \cos \theta_4 \right] \\ & - \left( \frac{c_9 - c_8}{c_7} L \right) \alpha_4 - \frac{c_8}{c_7} \ddot{l}_t \sin \theta_4 \end{aligned} \quad (3.38)$$

The equation is analysed by neglecting the dynamic term and solving for the quasi-static response using the following equation,

$$W(t) = \frac{f_1(t)\alpha_4 + f_2(t)\ddot{l}_t}{\omega_n^2 + f_3(t) + f_4(t)\ddot{l}_t} \quad (7.2)$$

where  $f_1(t)$  and  $f_2(t)$  are the coefficients of  $\alpha_4$  and  $\ddot{l}_t$  on the right hand-side of eq. (3.38), and  $f_4(t)$  is the last term in the coefficient

of  $W(t)$ . The quasi-static response is reduced by either decreasing the numerator or increasing the denominator by shaker excitation. However a decrease in the numerator does not necessarily increase the denominator because of the coupling of shaker inertial terms.

The flexural midspan deflection are measured perpendicular to the link in the plane of motion, the forcing fields imposed in this plane must be continuously modified in order to reduce the amplitude of deflection. This requires the absolute acceleration perpendicular to the link to be reduced. Fig. 7.6 shows the absolute acceleration  $a_{4a}$ , measured perpendicular to the rocker link in the plane of deflection; where it is a function of the inertial loading of the link as shown in eq. (7.3). Thus it is argued, if the magnitude of the absolute acceleration can be reduced by a viable shaker motion, then so too will the elastodynamic response, since the absolute acceleration terms provide the principal forcing functions.

$$a_{4a} = a_{4xy} \cos \theta$$

$$a_{4a} = f(r\alpha_4, r\omega_4^2, \ddot{l}_t) \cos \theta \quad (7.3)$$

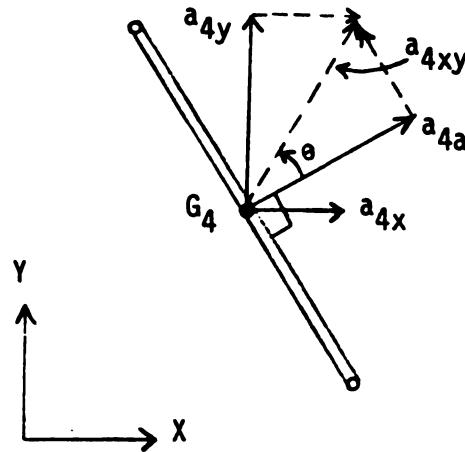











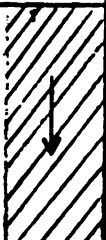



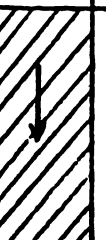


Fig. 7.6 : Absolute Acceleration of The Rocker Link

#### 7-2.2 SYNTHESIS OF SHAKER WAVEFORM

As discussed earlier in section 7-2.1, the profile of the link response will serve as a basis for the slider motion. Fig. 7.7 shows the analytical quasi-static response obtained at 200 rpm. Superimposed on it is the proposed shaker waveform, the shape being proportional to the deflection curve. Fig. 7.8 shows the computer simulation of the absolute acceleration of the rocker link corresponding to the proposed shaker waveform. It shows a decrease in magnitude in the first half-cycle and an increase in the second half-cycle, so does the elastodynamic response as shown in Fig. 7.9. An experimental investigation was carried out by feeding the experimental quasi-static response curve into the shaker simultaneously with crank motion. The result is shown in Fig. 7.10,

which correlates with the analytical result. Fig. 7.11 shows the angular acceleration of the rocker link.

Fig. 7.12 shows the inverse of the quasi-static response as being the proposed shaker waveform. The results corresponding to this waveform are shown in Figures 7.13, 7.14, 7.15 and 7.16. The results obtained for two different sets of shaker waveform are summarized in Table 7.1.

	Analytical						Experimental	
	absolute acceleration $a_{a4}$		angular acceleration $\alpha_4$		deflection of link		deflection of link	
	1 <sup>st</sup> half	2 <sup>nd</sup>	1 <sup>st</sup> half	2 <sup>nd</sup>	1 <sup>st</sup> half	2 <sup>nd</sup>	1 <sup>st</sup> half	2 <sup>nd</sup>
shaker waveform proportional to link deflection								
shaker waveform is inverse of link deflection								

↑ increase in magnitude  
↓ decrease in magnitude

Table 7.1 : Variation of link response with shaker at 200 rpm

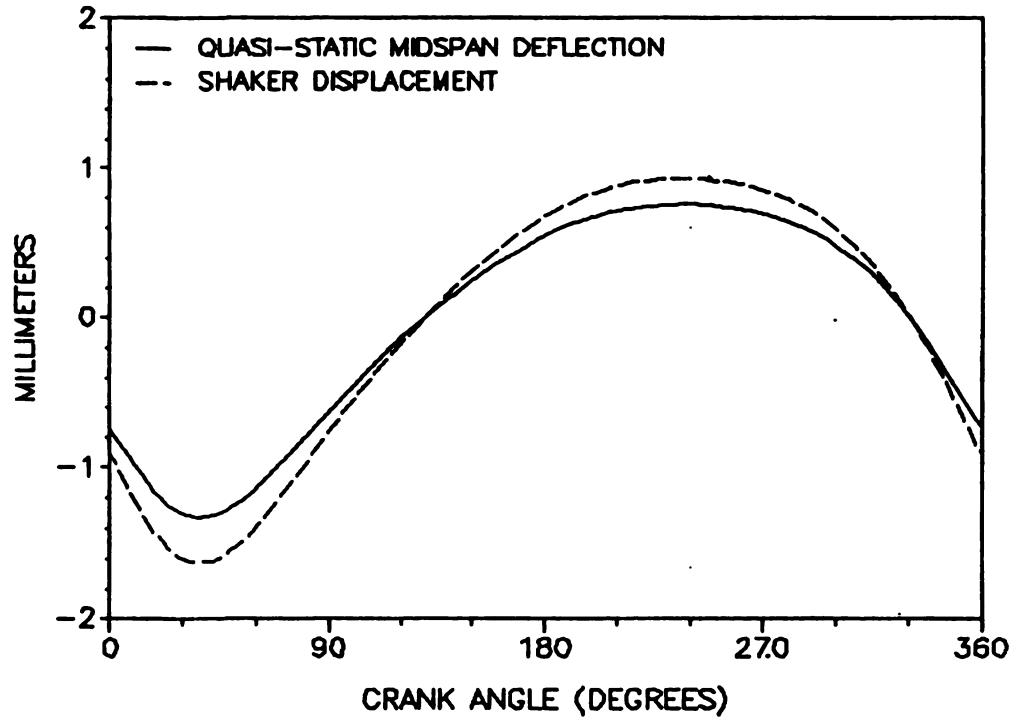


Fig. 7.7 : Suggested shaker/slider waveform proportional to quasi-static response

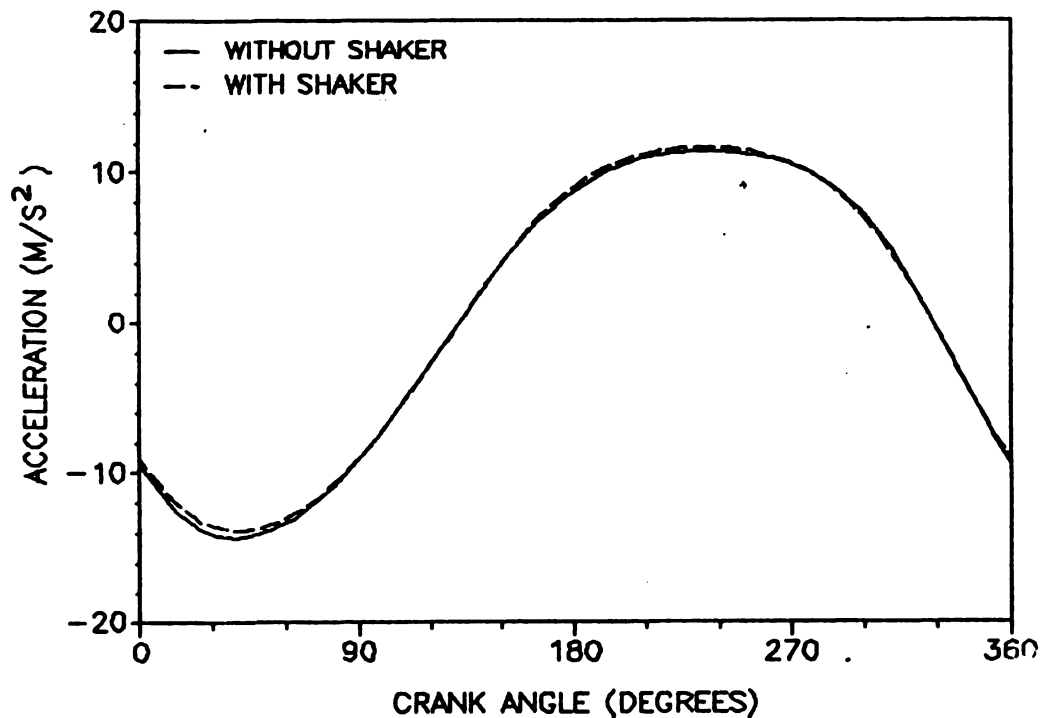


Fig. 7.8 : Absolute acceleration of the rocker link at 200 rpm given shaker/slider waveform shown in Fig. 7.7

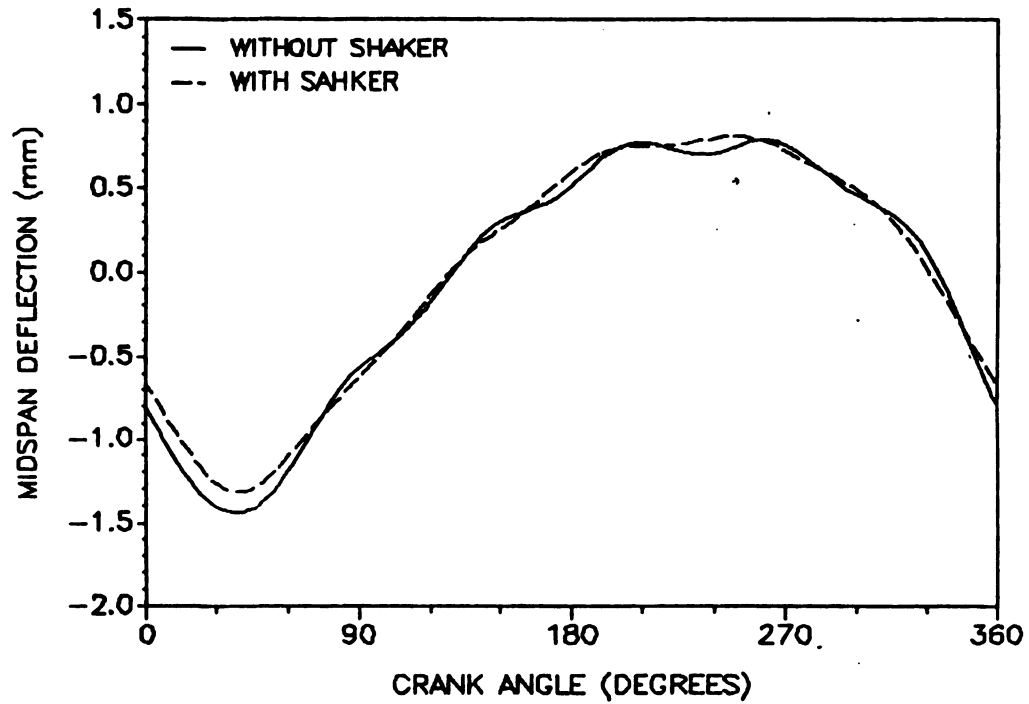


Fig. 7.9 : Analytical elastodynamic response at 200 rpm  
given shaker/slider waveform shown in Fig. 7.7

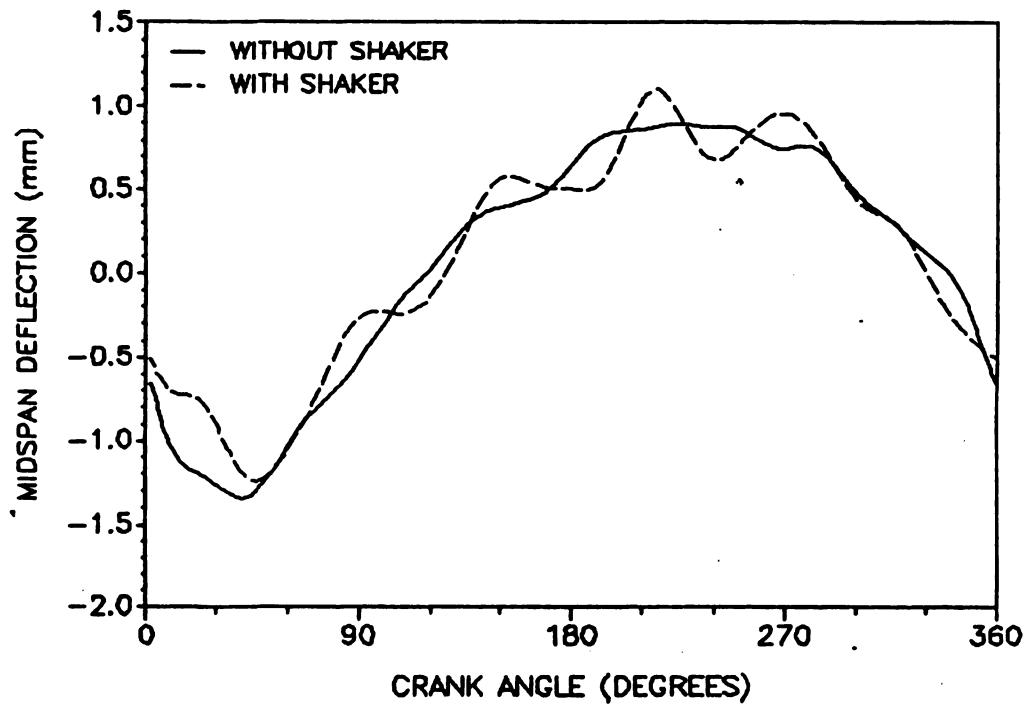


Fig. 7.10 : Experimental elastodynamic response at 200 rpm  
given shaker/slider waveform shown in Fig. 7.7

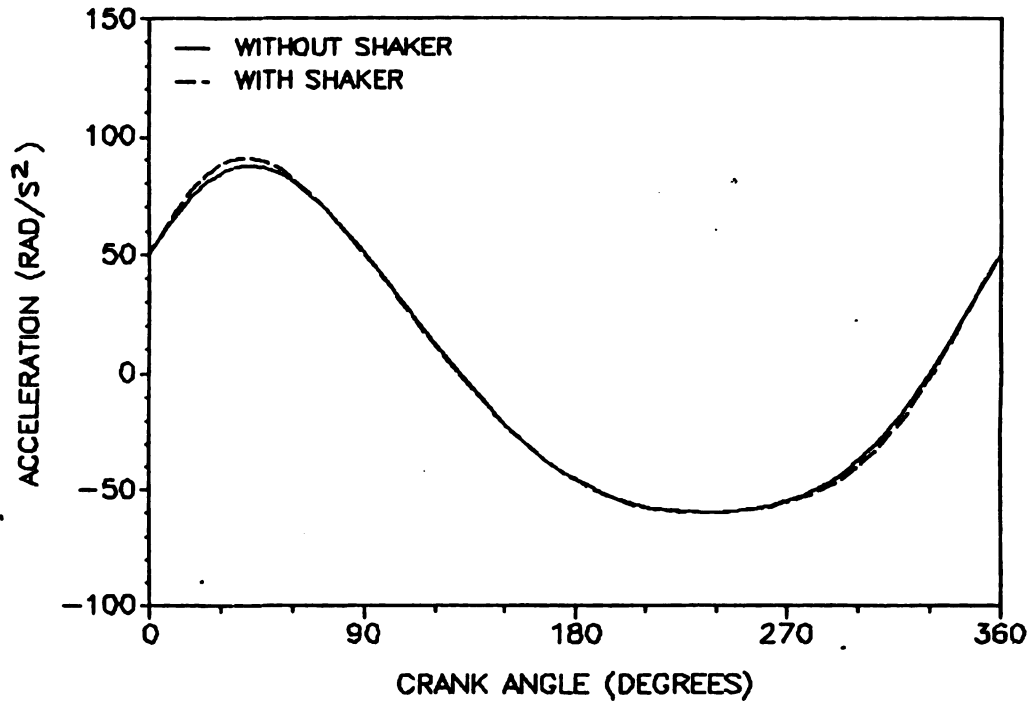


Fig. 7.11 : Angular acceleration of the rocker link at 200 rpm  
given shaker/slider waveform shown in Fig. 7.7

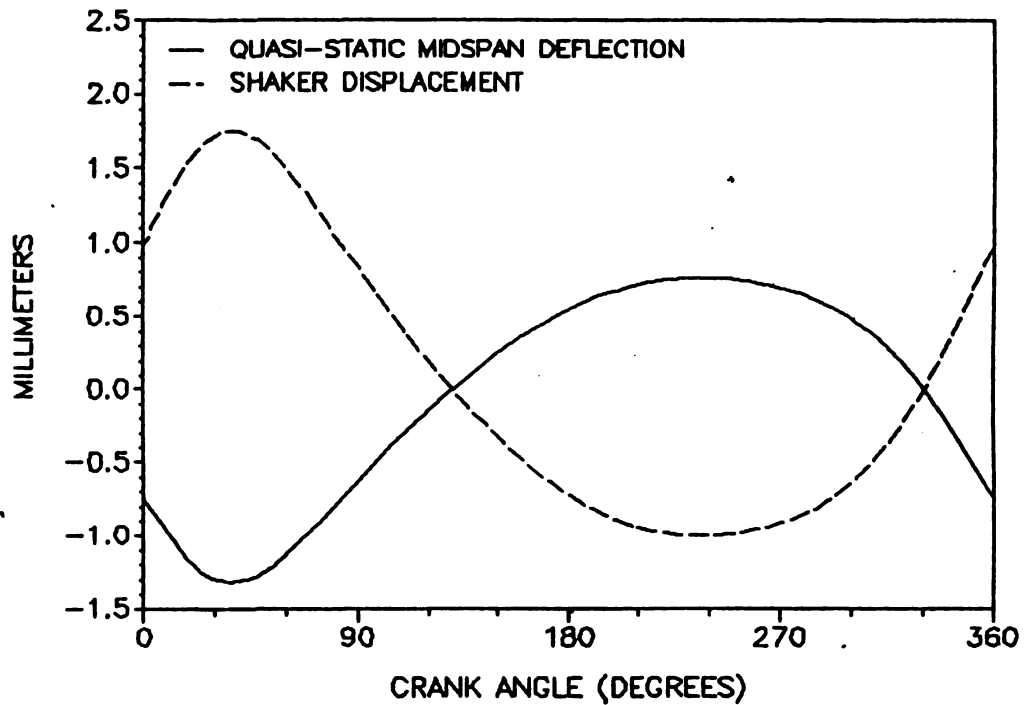


Fig. 7.12 : Suggested shaker/slider waveform inverse  
of quasi-static response

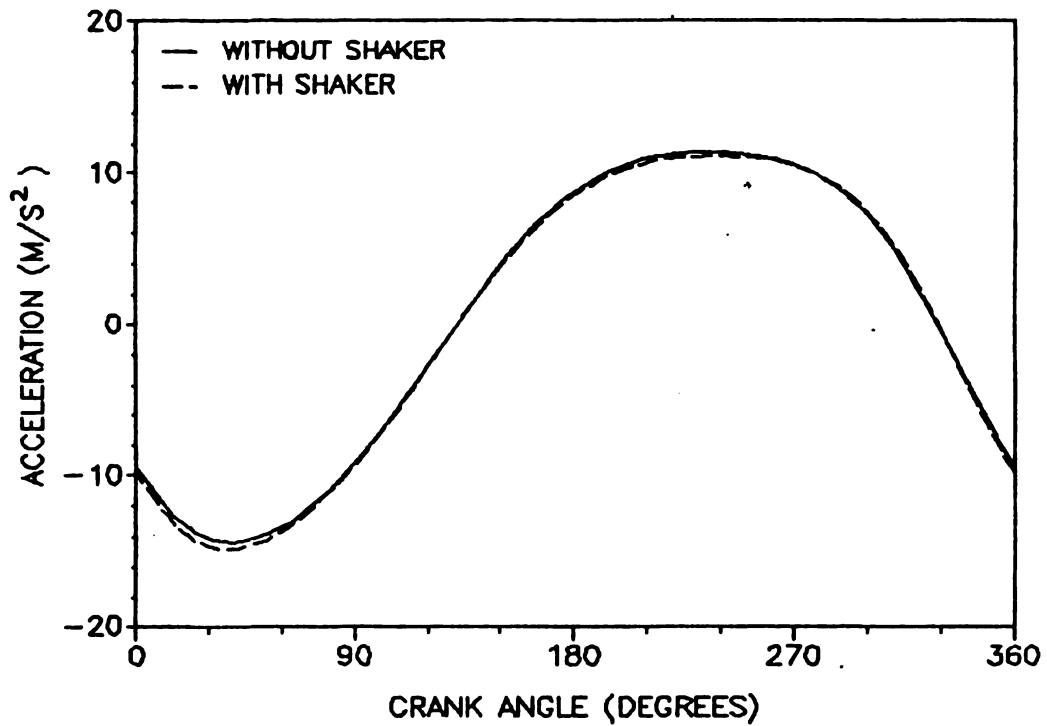


Fig. 7.13 : Absolute acceleration of rocker link at 200 rpm  
given shaker/slider waveform shown in Fig. 7.12

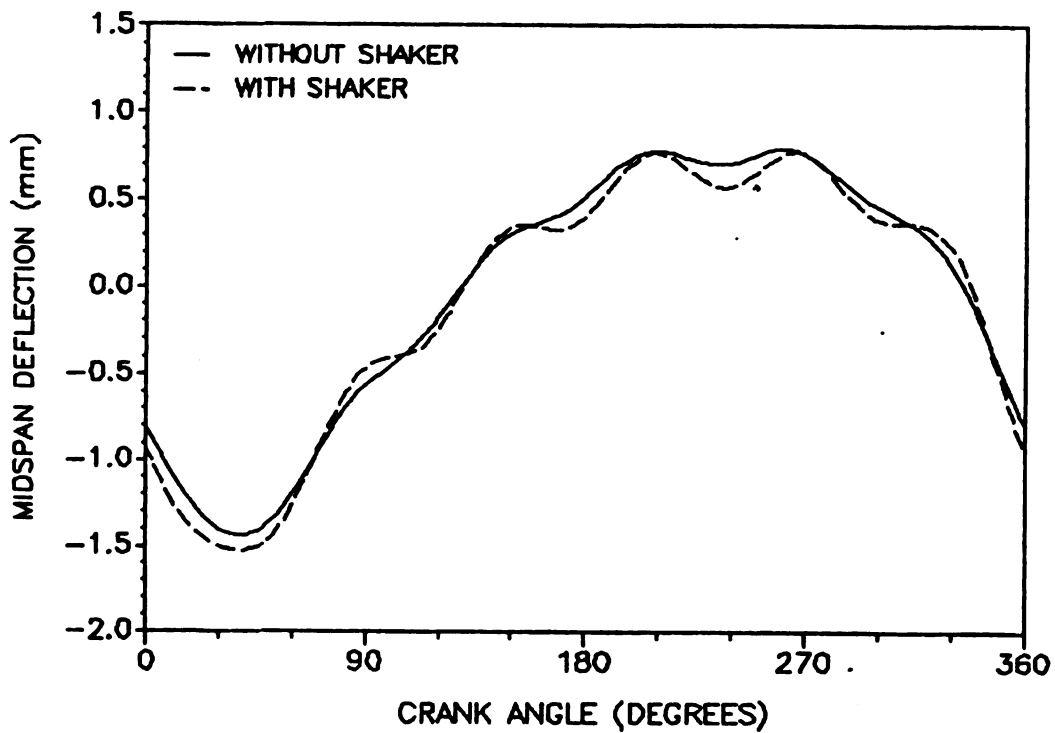


Fig. 7.14 : Analytical elastodynamic response at 200 rpm  
given shaker/slider waveform shown in Fig. 7.12





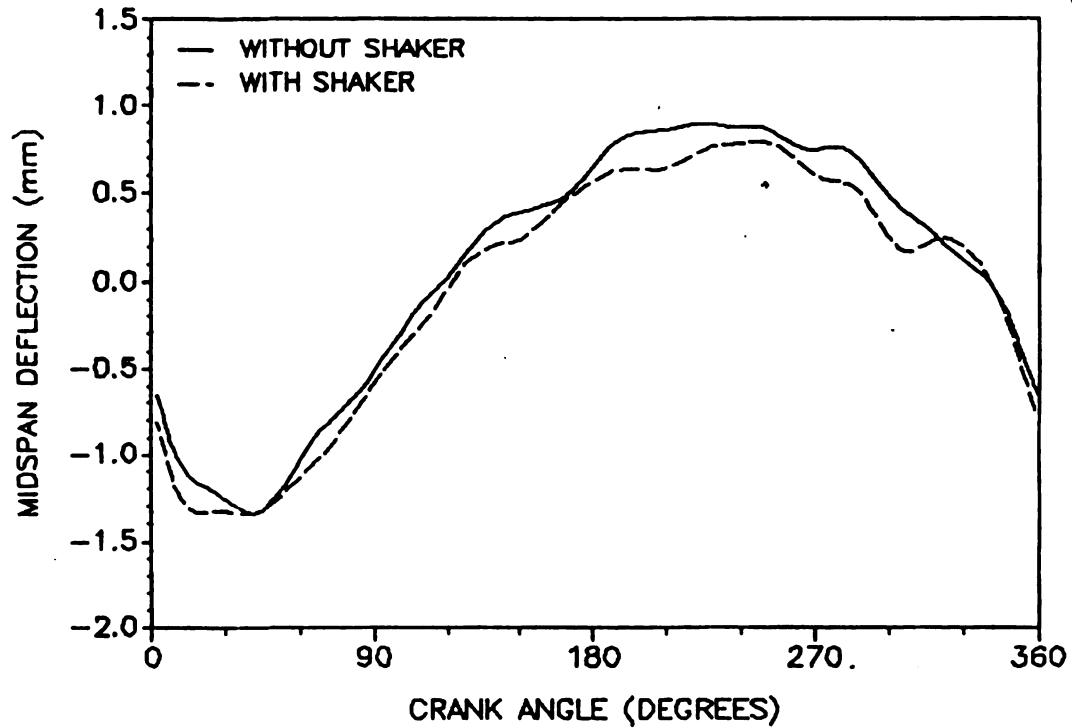


Fig. 7.15 : Experimental elastodynamic response at 200 rpm  
given shaker/slider waveform shown in Fig. 7.12

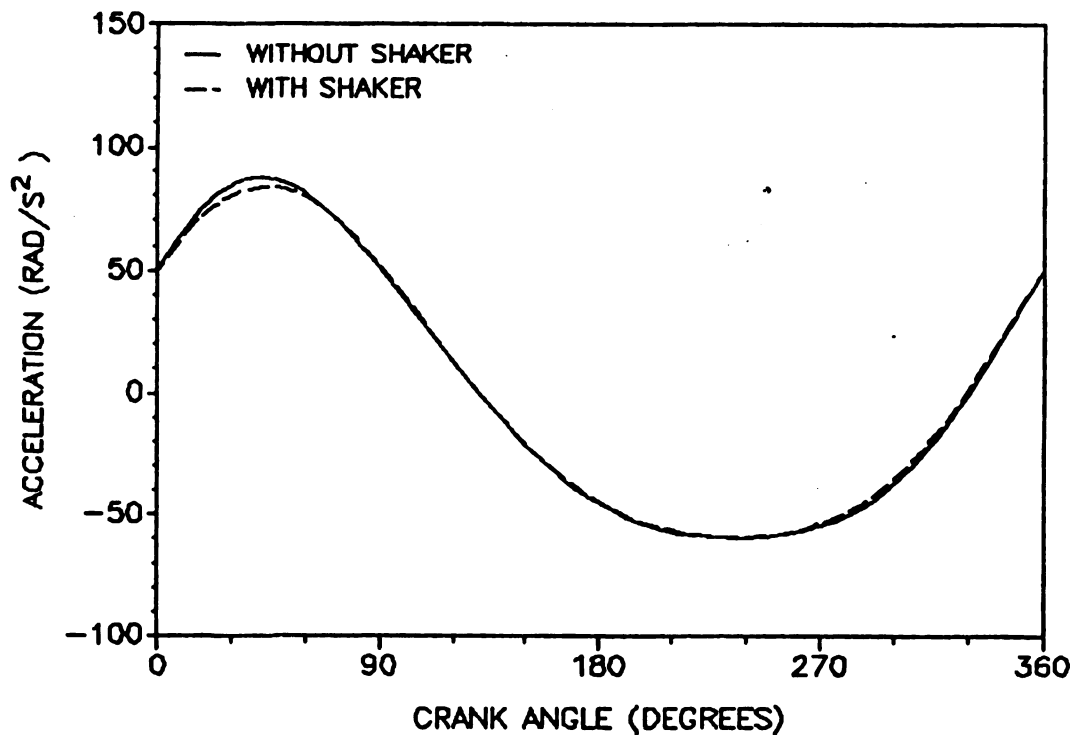


Fig. 7.16 : Angular acceleration of the rocker link at 200 rpm  
given shaker/slider waveform shown in Fig. 7.16

Both experimental and analytical link deflections are dependent on the absolute acceleration of the link. Note that a decrease in angular acceleration of the link does not necessarily reduce the deflection.

The data from Table 7.1 implies that the peak response in both halves of the cycle may be reduced by having a shaker waveform proportional to link deflection in the first half and a waveform inverse of the link deflection in the second half. This notion is graphically shown in Fig. 7.17, where discontinuities on the curve occur due to the inversion process. From the experimental point of view, excitation of the shaker with a discontinuous waveform may result in erroneous slider motion (displacement with spikes), which is not recommended [27]. This can be avoided by smoothing the discontinuities as shown by the modified curve. This general approach is accomplished for any operating speed by feeding the modified experimental quasi-static response data to the arbitrary waveform generator which provides the excitation for the shaker. The shaker must be carefully orchestrated with the primary forcing function provided by the crank motion in order to reduce the elastodynamic response of the rocker link.

This waveform will serve as a possible optimum curve for the slider motion. In this fashion, the shaker frequency would be the same as crank frequency and the phase would be zero. The only unknown is the slider amplitude, which has a constraint of  $\pm 8$  mm. If this waveform can reduce the absolute acceleration of the rocker link, then it may be justified that it will in turn reduce the link deflection. As it turns out, it does behave accordingly and the results are shown in the next chapter.

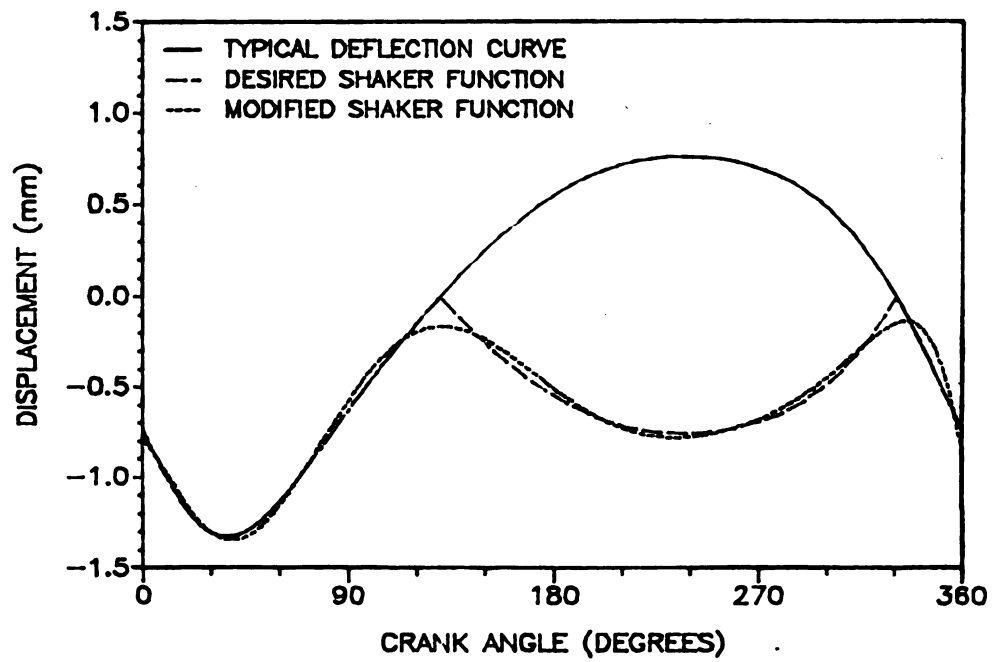


Fig. 7.17 : Synthesis of Shaker/slider Waveform

## **CHAPTER 8**

### **EXPERIMENTAL & COMPUTATIONAL RESULTS**

In chapter 7, section 7-1, the analytical deflection of the rocker link of a classical four-bar linkage was shown to correlate with the experimental results. Having defined the shaker waveform, computer simulation and experimental investigation were carried out by exciting the shaker simultaneously with crank motion. The results are presented for crank frequency of 148, 170, 200 and 215 rpm.

#### **8-1 RESPONSE DATA & ABSOLUTE ACCELERATION OF THE FLEXIBLE LINK**

The experimental elastodynamic and quasi-static midspan deflection at 148 rpm are shown in Figs. 8.1 and 8.2 respectively, followed by analytical results in Figs. 8.3 and 8.4. The absolute acceleration at 148 rpm is shown in Fig. 8.5.

The experimental and analytical response at 170 rpm is shown in Figs. 8.6 and 8.7 respectively, followed by absolute acceleration in Fig. 8.8. The results at 200 rpm are shown in Figs. 8.9 to 8.11. A comparison of experimental and analytical result for the intelligent mechanism at 200 rpm is shown in Fig. 8.12. Figs. 8.13 to 8.16 present the results at 215 rpm

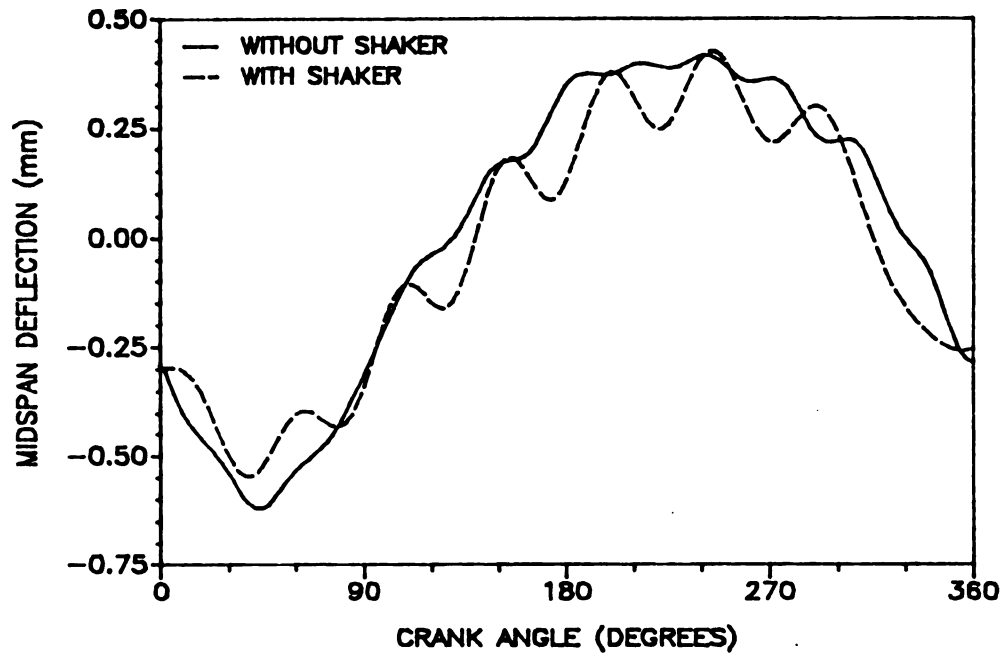


Fig. 8.1 : Experimental elastodynamic response at 148 rpm

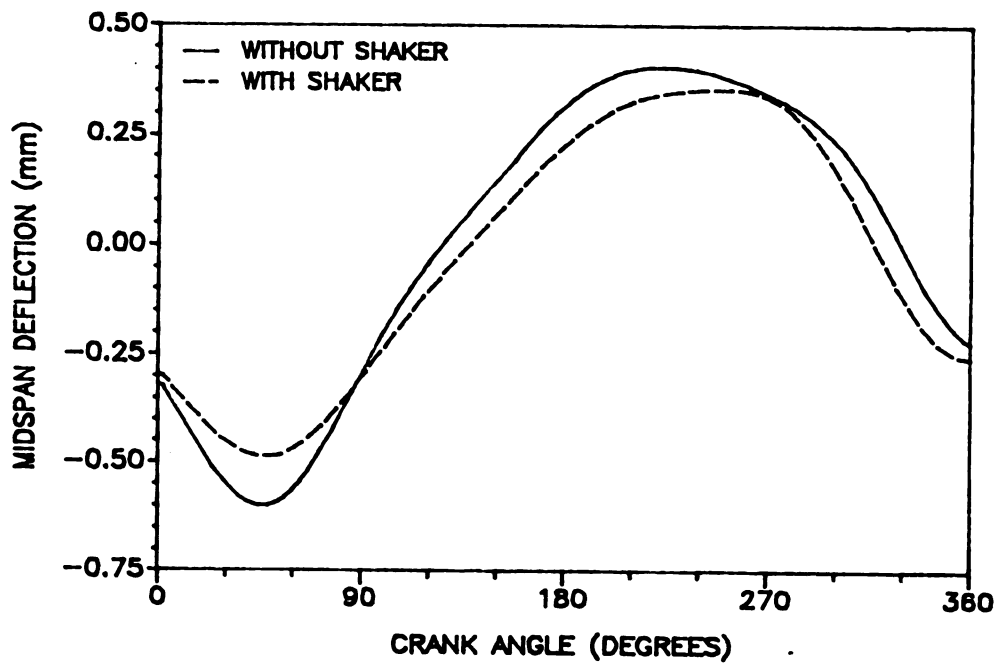


Fig. 8.2 : Experimental quasi-static response at 148 rpm

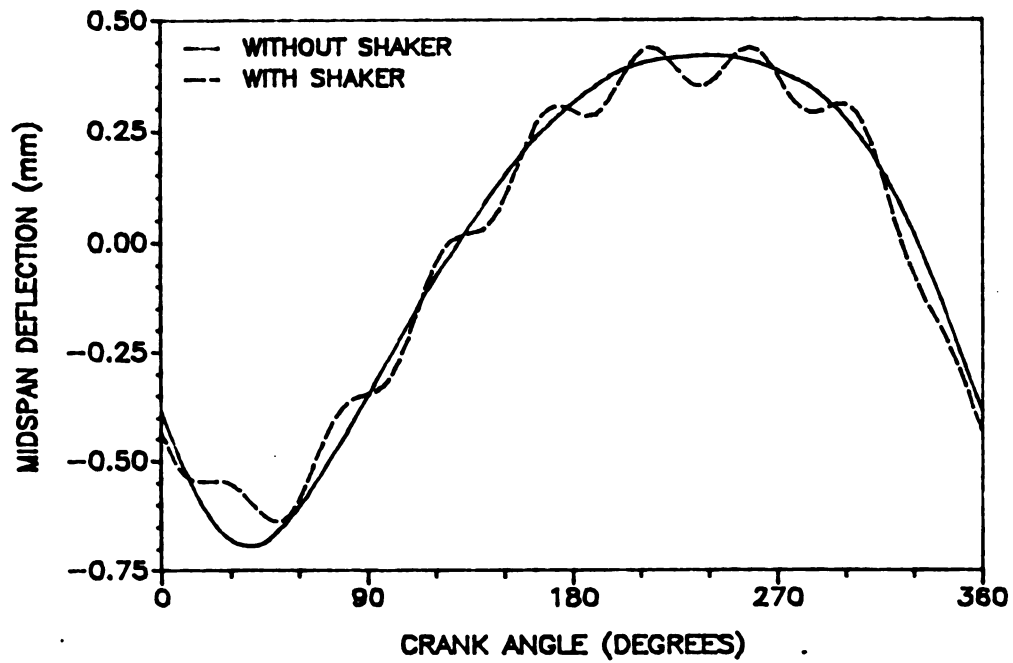


Fig. 8.3 : Analytical elastodynamic response at 148 rpm

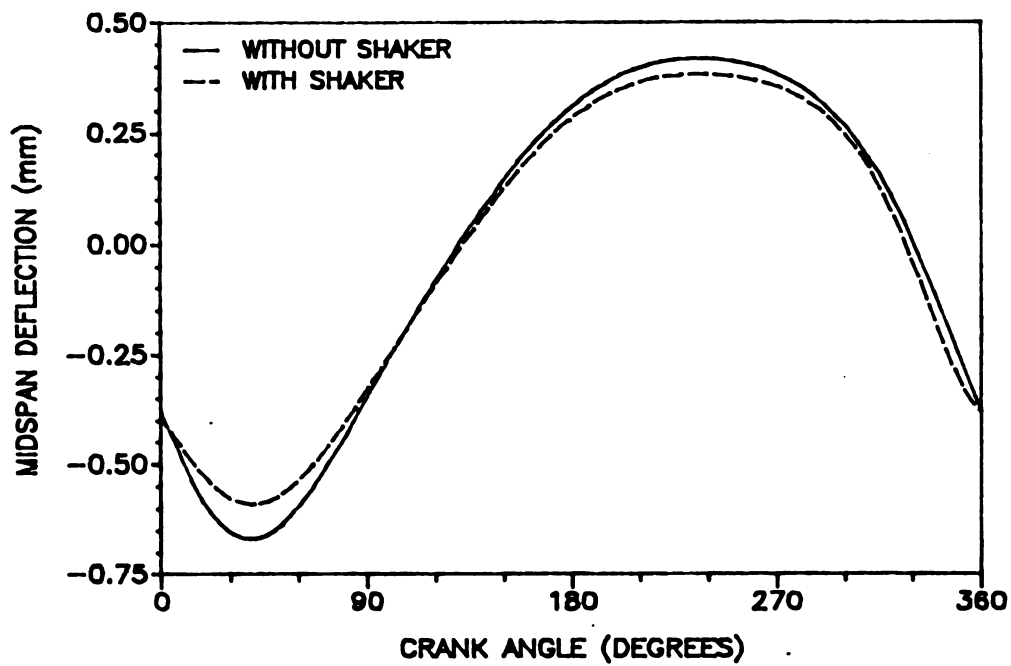


Fig. 8.4 : Analytical quasi-static response at 148 rpm

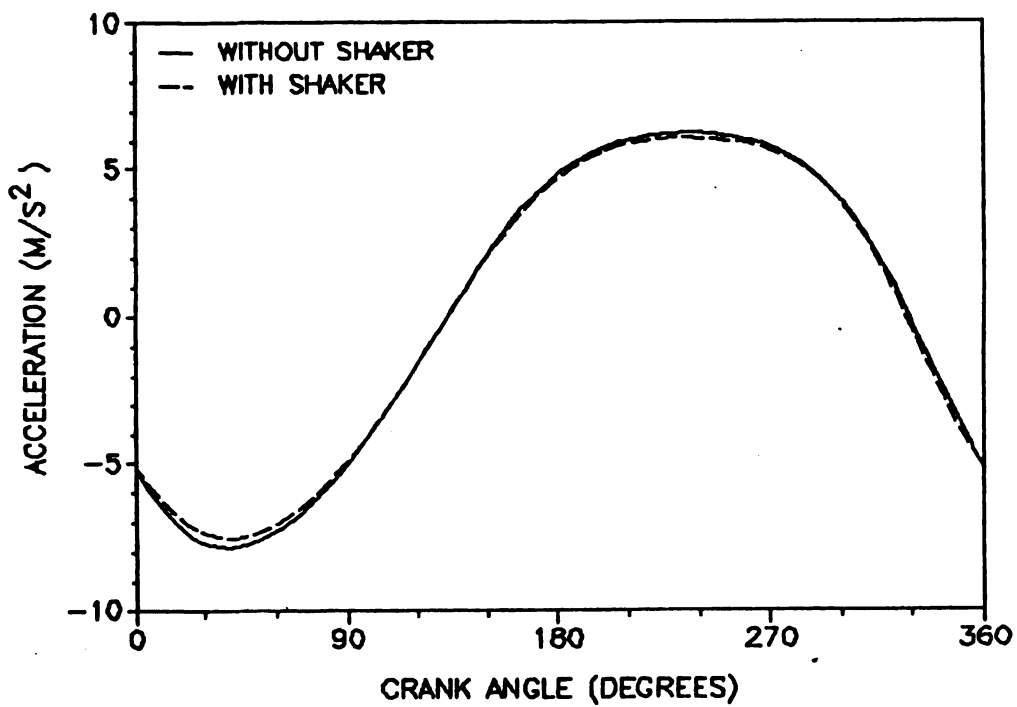


Fig. 8.5 : Absolute acceleration of the rocker link at 148 rpm

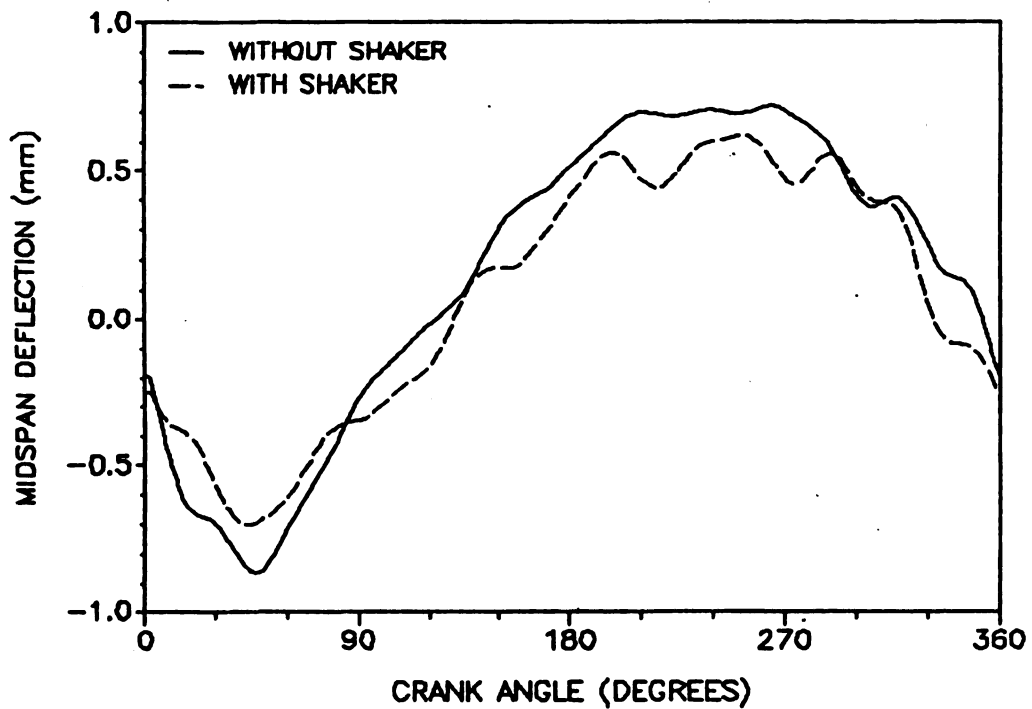


Fig. 8.6 : Experimental elastodynamic response at 170 rpm



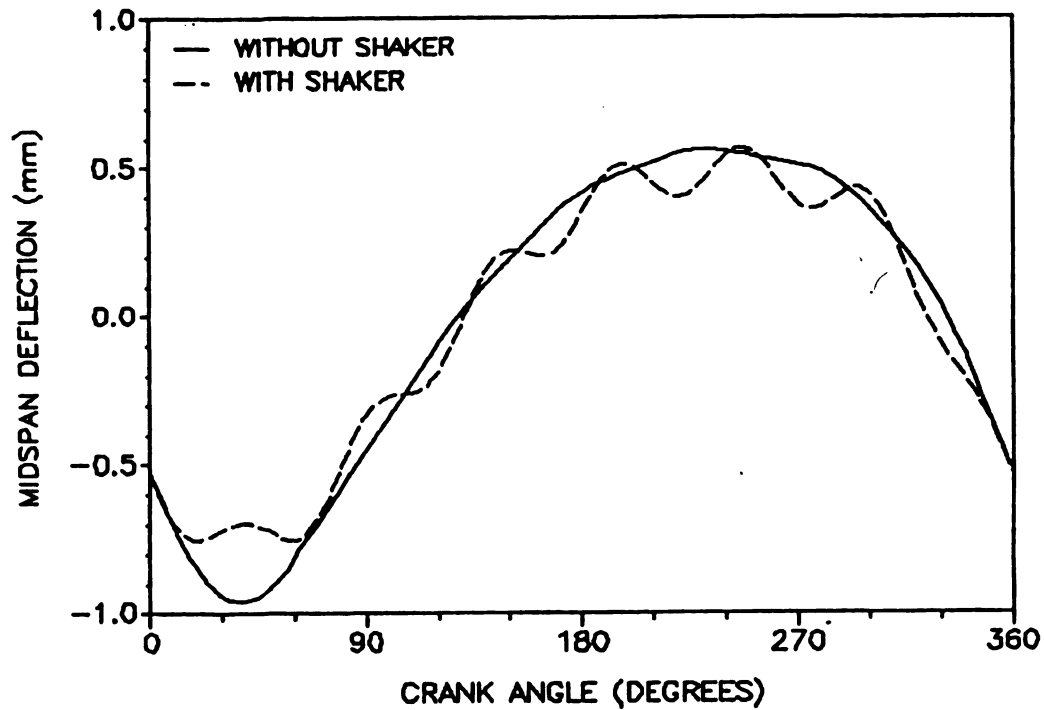


Fig. 8.7 : Analytical elastodynamic response at 170 rpm

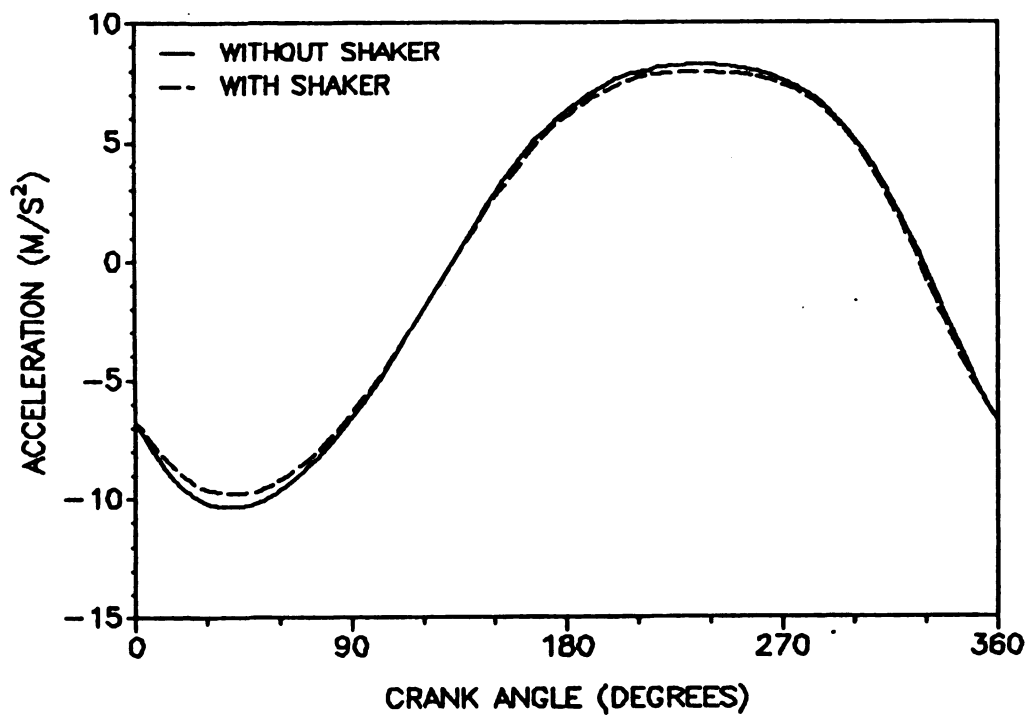


Fig. 8.8 : Absolute acceleration of the rocker link at 170 rpm

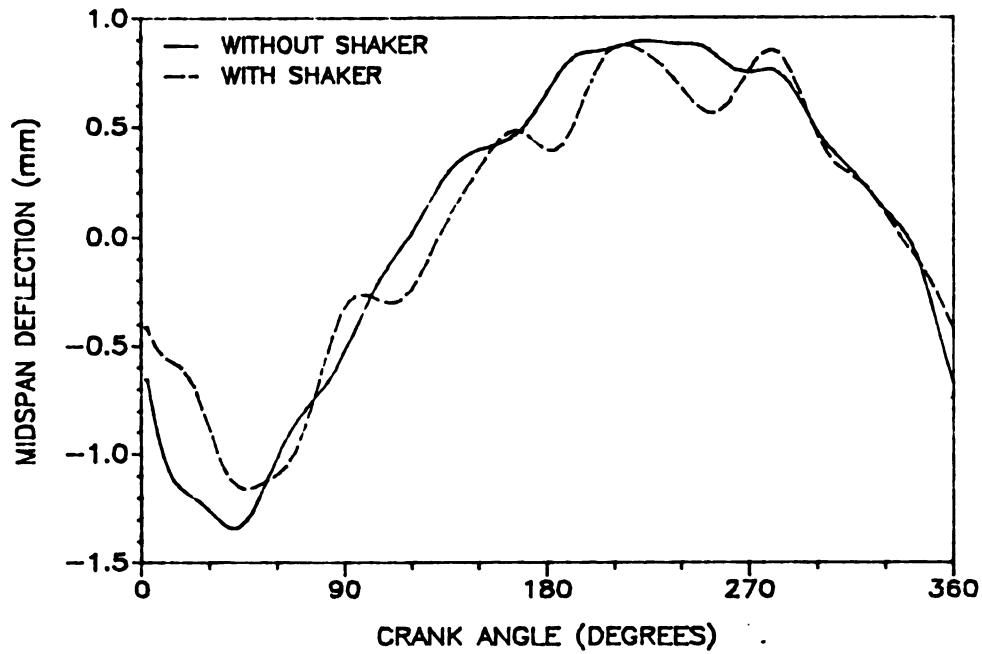


Fig. 8.9 : Experimental elastodynamic response at 200 rpm

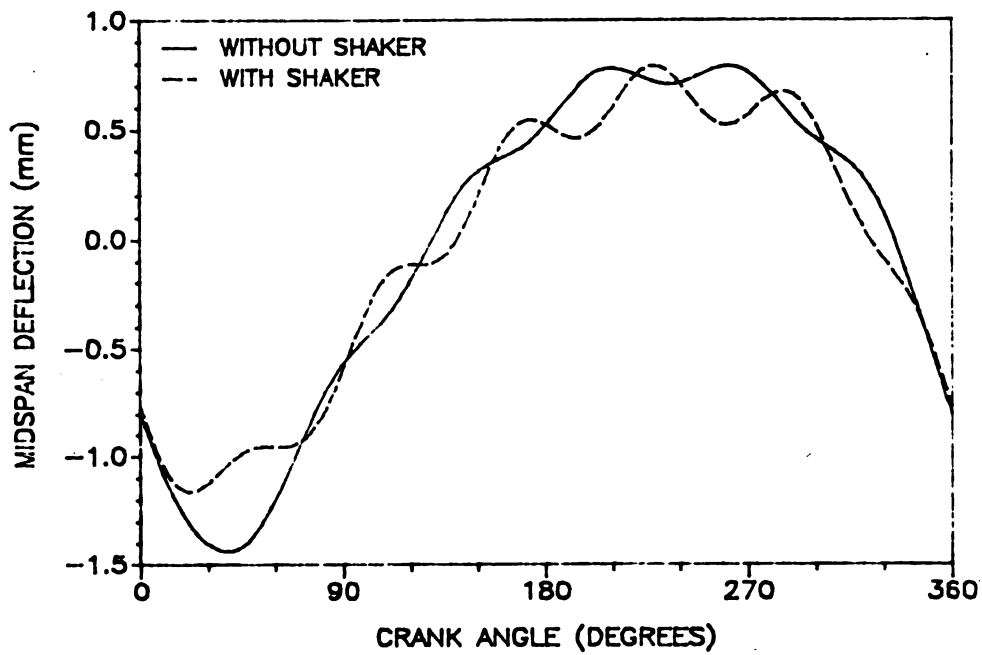


Fig. 8.10 : Analytical elastodynamic response at 200 rpm

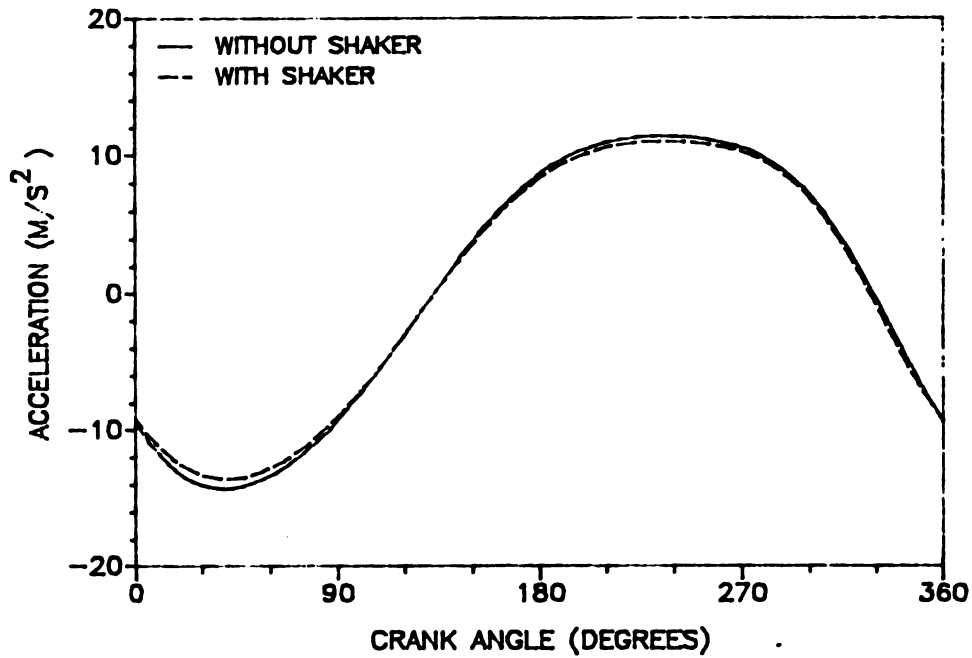


Fig. 8.11 : Absolute acceleration of the rocker link at 200 rpm

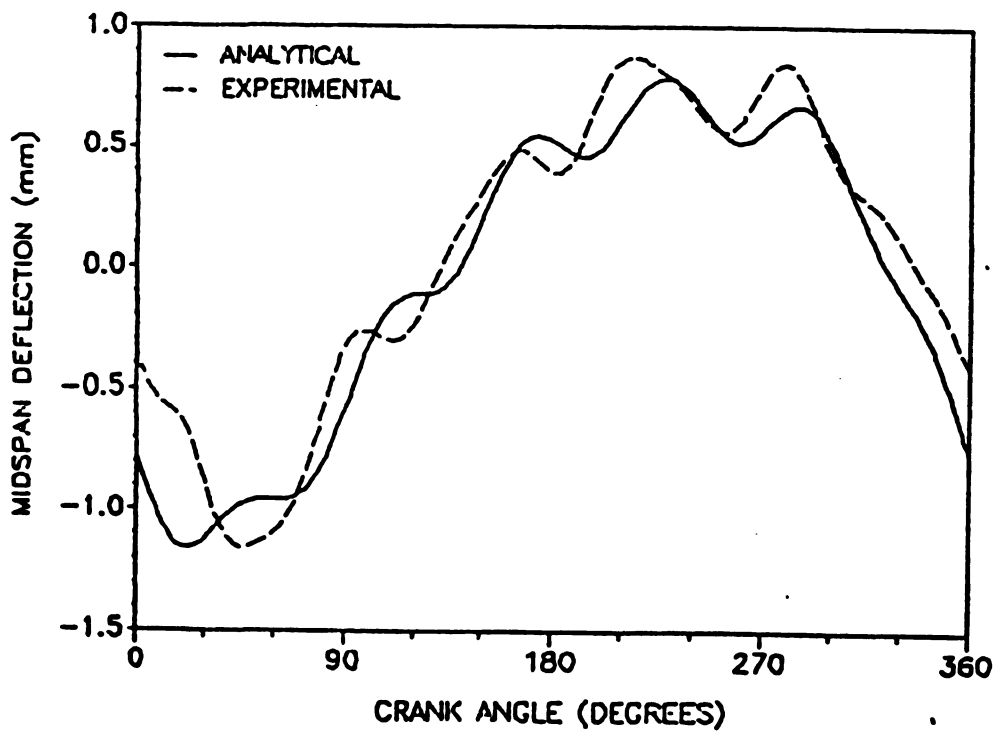


Fig. 8.12 : Analytical and experimental results for the intelligent mechanism at 200 rpm

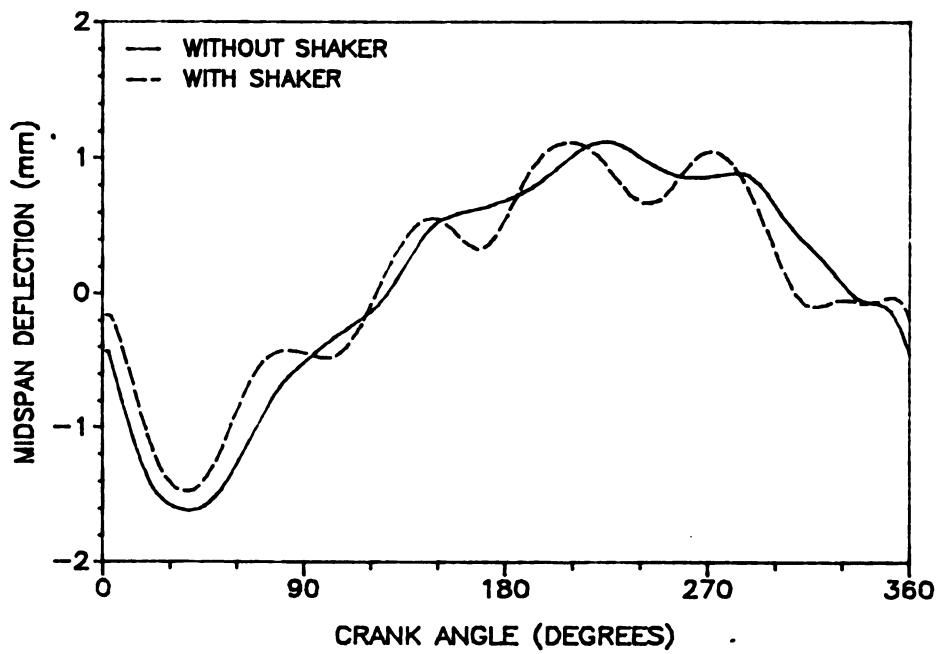


Fig. 8.13 : Experimental elastodynamic response at 215 rpm

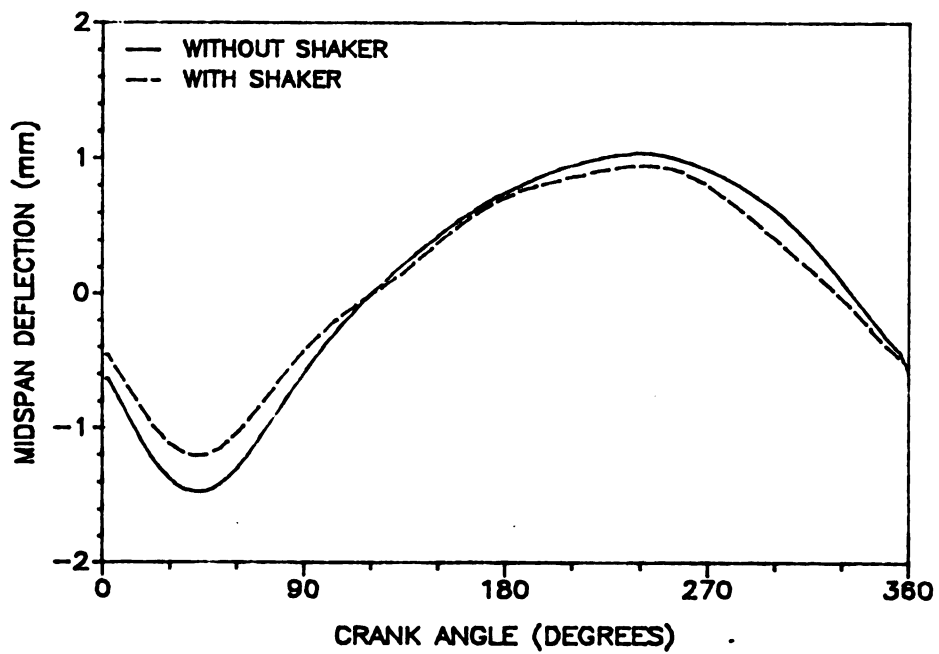


Fig. 8.14 : Experimental quasi-static response at 215 rpm

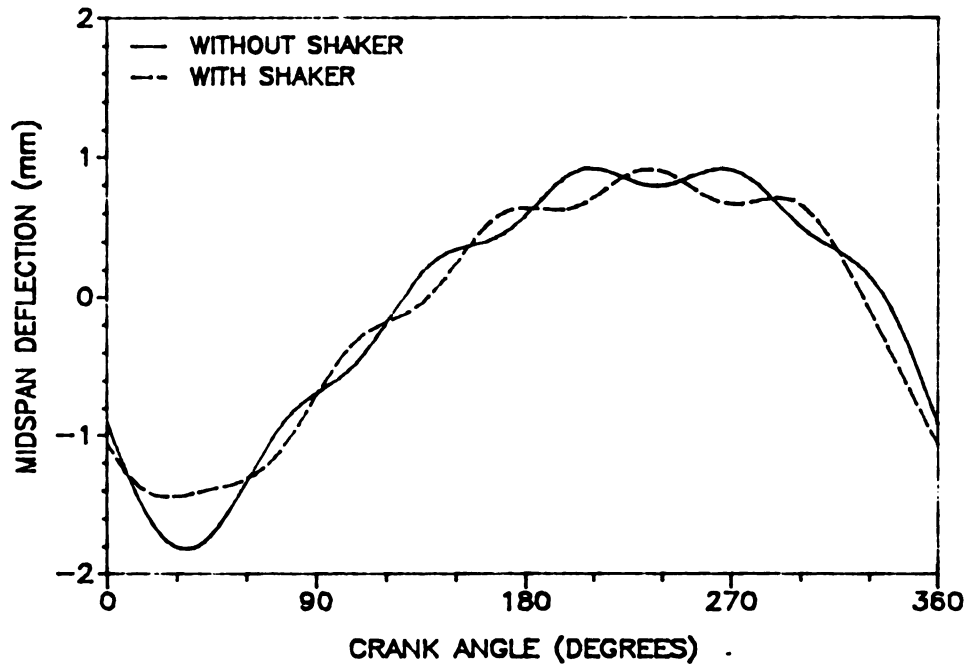


Fig. 8.15 : Analytical elastodynamic response at 215 rpm

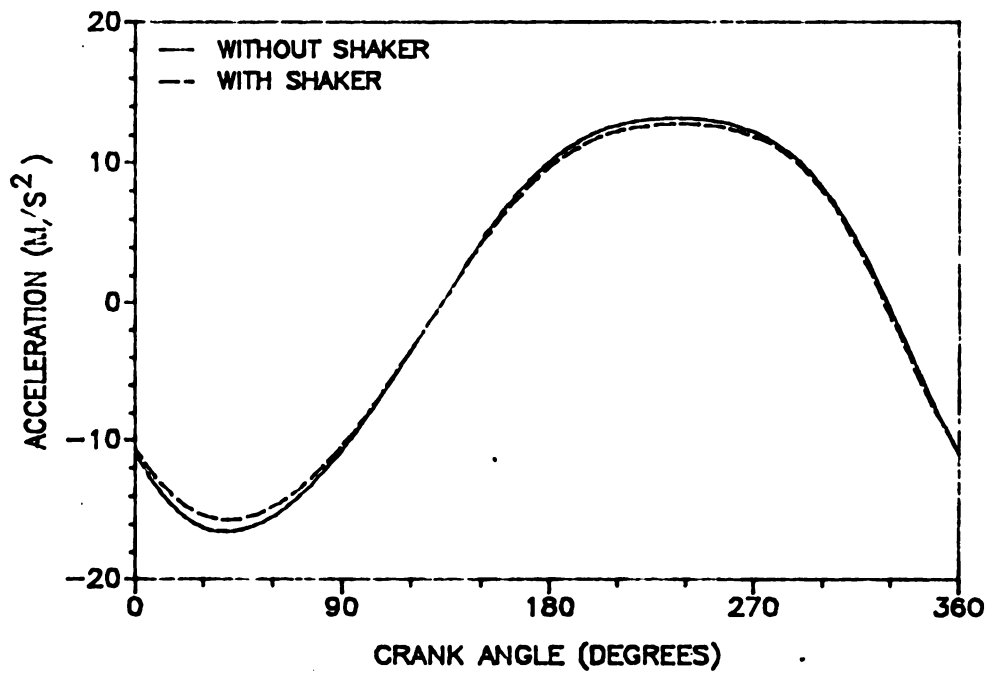


Fig. 8.16 : Absolute acceleration of the rocker link at 215 rpm

**8-2 KINEMATIC RESULTS FOR THE FLEXIBLE LINK**

The analytical and experimental slider displacement, velocity and acceleration are compared in Figures 8.17 to 8.28. The force exerted by the shaker on the slider are shown in Figs. 8.29 to 8.32. The simulation of angular acceleration of the rocker link are shown in Figs. 8.33 to 8.36

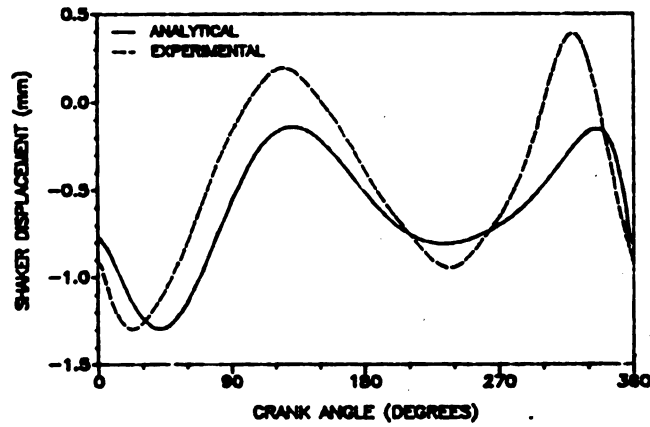


Fig. 8.17 : Shaker/slider displacement at 148 rpm

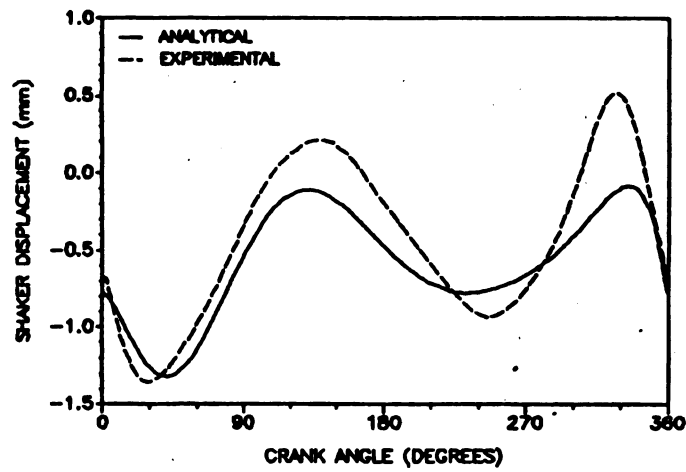


Fig. 8.18 : Shaker/slider displacement at 170 rpm

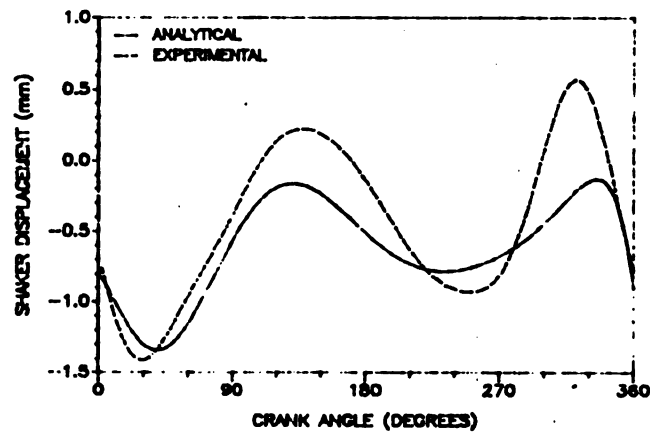


Fig. 8.19 : Shaker/slider displacement at 200 rpm

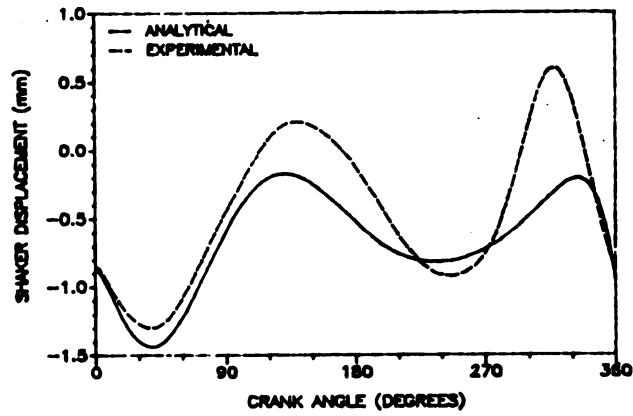


Fig. 8.20 : Shaker/slider displacement at 215 rpm

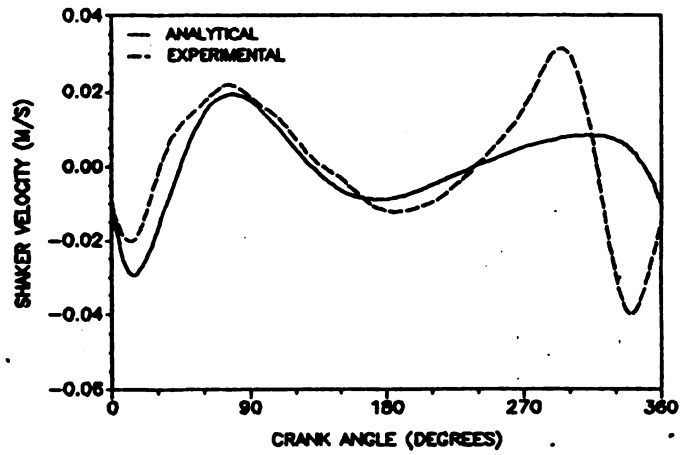


Fig. 8.21 : Shaker/slider velocity at 148 rpm

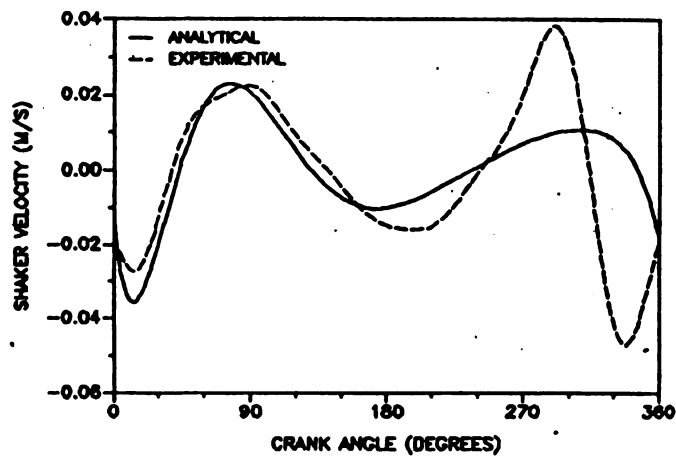


Fig. 8.22 : Shaker/slider velocity at 170 rpm



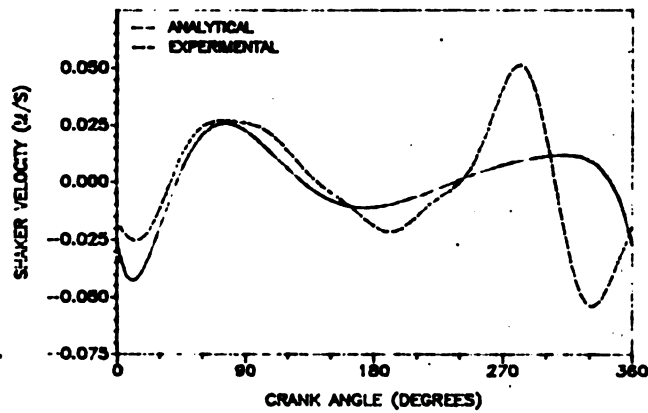


Fig. 8.23 : Shaker/slider velocity at 200 rpm

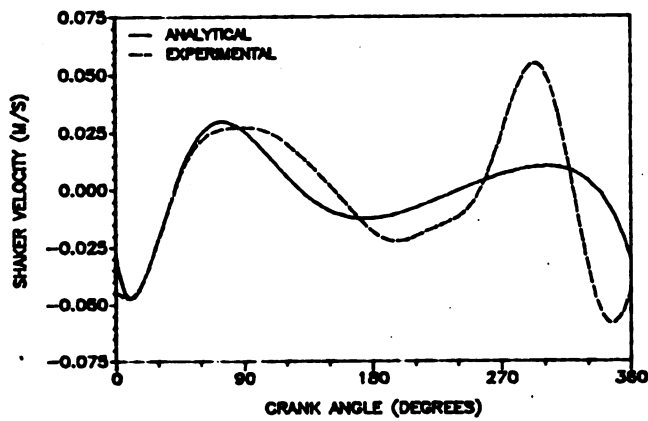


Fig. 8.24 : Shaker/slider velocity at 215 rpm

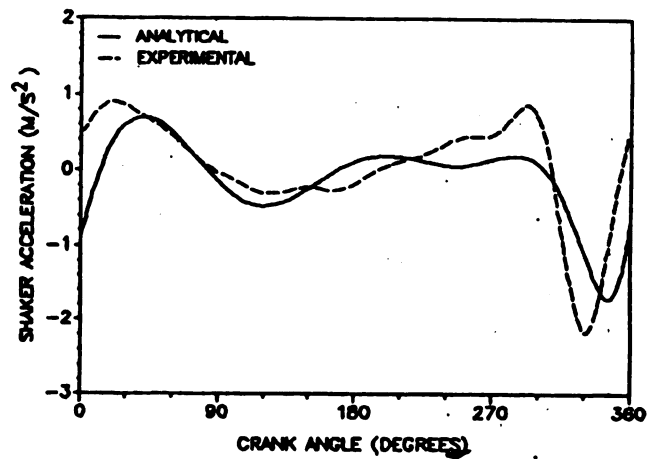


Fig. 8.25 : Shaker/slider acceleration at 148 rpm

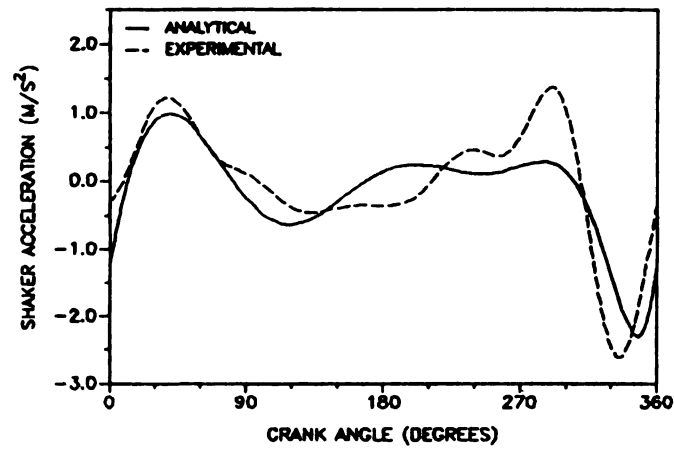


Fig. 8.26 : Shaker/slider acceleration at 170 rpm

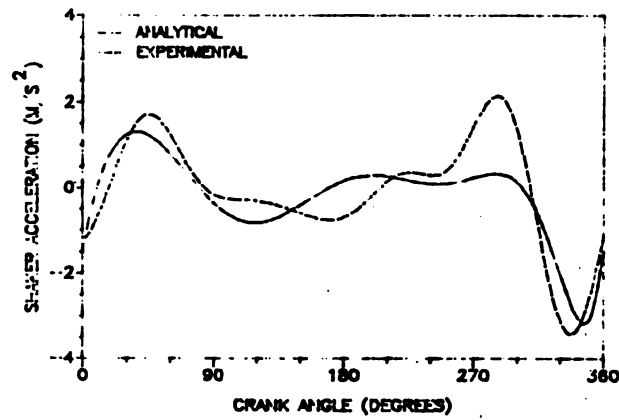


Fig. 8.27 : Shaker/slider acceleration at 200 rpm

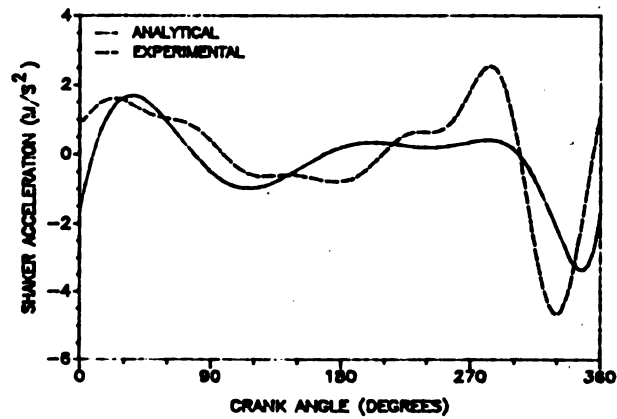


Fig. 8.28 : Shaker/slider acceleration at 215 rpm

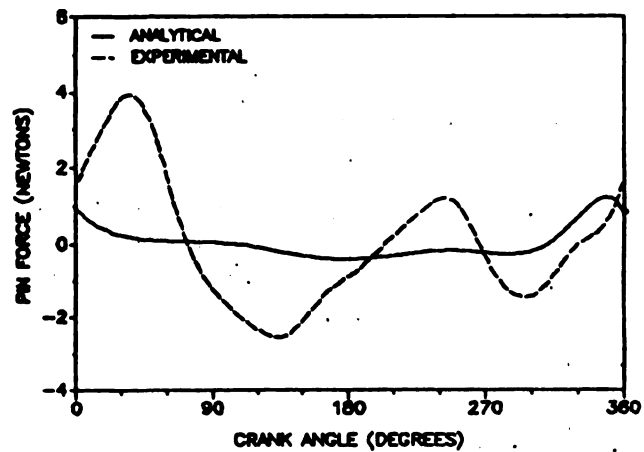


Fig. 8.29 : Force exerted by the shaker on the slider at 148 rpm

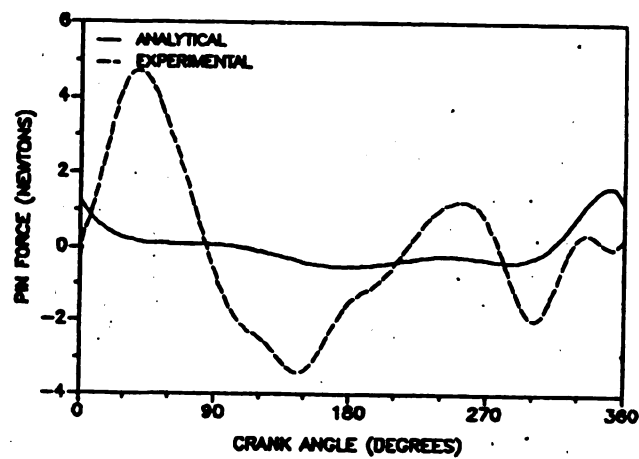


Fig. 8.30 : Force exerted by the shaker on the slider at 170 rpm

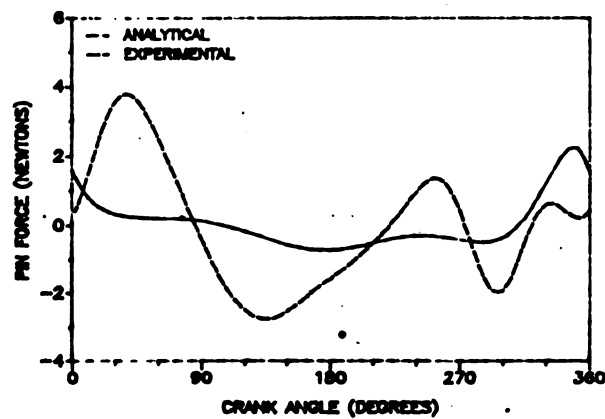


Fig. 8.31 : Force exerted by the shaker on the slider at 200 rpm

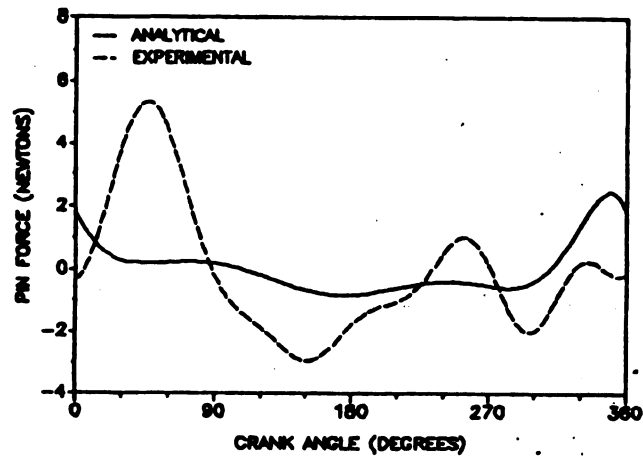


Fig. 8.32 : Force exerted by the shaker on the slider at 215 rpm

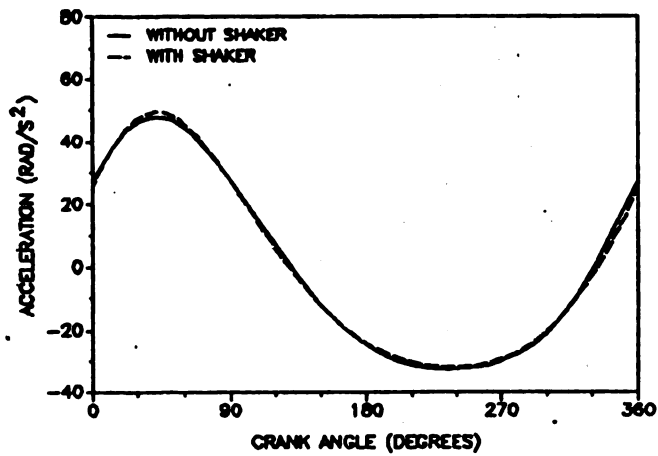


Fig. 8.33 : Angular acceleration of the rocker link at 148 rpm

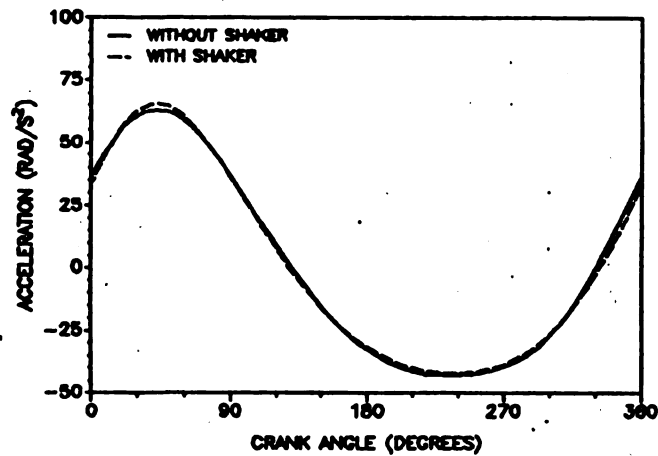


Fig. 8.34 : Angular acceleration of the rocker link at 170 rpm

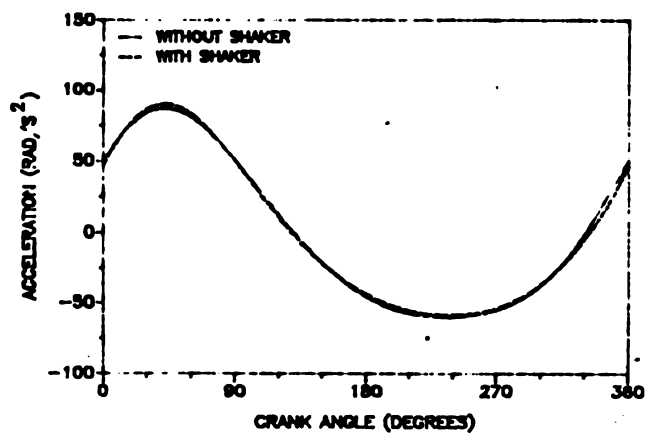


Fig. 8.35 : Angular acceleration of the rocker link at 200 rpm

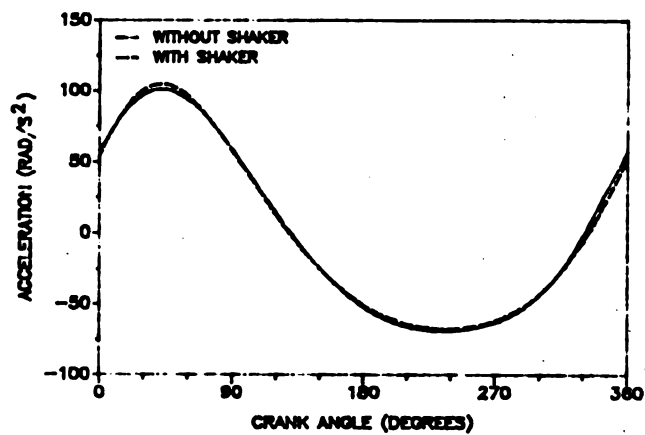


Fig. 8.36 : Angular acceleration of the rocker link at 215 rpm

## CHAPTER 9

### DISCUSSION OF RESULTS

Figures 7.1 to 7.4 in chapter 7 show that the correlation between analytical and experimental elastodynamic response of a four-bar linkage are extremely good, thus proving that appropriate approximating statements have been introduced into the variational formulation and correct solution procedure has been utilized by the principal of normal modes.

The experimental elastodynamic response at 148 rpm in Fig. 8.1 shows a reduction of 12% in the first half-cycle, but the amplitude remains more or less the same in the second half-cycle. Since the fundamental response curve has a larger peak amplitude in the first half-cycle than in second half of the cycle (for all operating speed), a reduction in the first half would be a important design consideration. The experimental response at 170 rpm (Fig. 8.6) shows by far the best result with a 19% reduction in amplitude in the first half-cycle and 11% reduction in the second half-cycle. The response curves at 200 rpm (Fig. 8.9) and 215 rpm (Fig. 8.13) shows a reduction of 15% and 7% respectively, but the amplitude remains more or less the same in the second half of the cycle. The analytical elastodynamic response predicts a reduction in amplitude in the first half of the cycle, even though the accompanying absolute acceleration is reduced at both peaks for all operating speeds. Plausible explanations for this behaviour will now be presented.

Firstly, in the curve synthesis of shaker, it was shown that a

waveform with inverse of a deflection curve gave a reduction in absolute acceleration and midspan deflection in the second half of response curve. Hence, final waveform was modified by inversion and smoothing. This process changed the boundary conditions of the shaker motion and consequently the kinematic characteristics are altered slightly. Secondly, damping was neglected in the derivation of the equations of motion, which resulted in larger vibrational amplitude. Finally the kinematic analysis does not incorporate the flexible body, i.e. the analysis is based on rigid-body.

Fig. 8.12 presents analytical and experimental response curves at 200 rpm, which validate the models developed for this class of machinery. The quasi-static response from analytical and experimental investigation shows reduction through the cycle for all operating speeds.

The experimental and analytical shaker displacement data are shown in Figs. 8.17-8.20. There is a slight discrepancy between the analytical and experimental results. All the experimental results tend to show a d.c. offset above the zero axis line in comparison to the analytical results. From the experimental point of view, the shaker always tends to move symmetrically and it is very difficult to keep the motion below the neutral line. The shaker velocity is compared in Figs. 8.21-8.24 and the acceleration are shown in Figs. 8.25-8.28. A reasonable correlation exists between the analytical and experimental results, even though it is difficult to excite the shaker in a prescribed manner.

The theoretical and experimental force exerted by the shaker on the slider are compared in Figs. 8.29-8.32. A comparable difference exists between the two solutions. The possible explanations are: 1) the force analysis was undertaken assuming the links are rigid-bodies, even though the rocker link is flexible; 2) the electrodynamic vibrator might not be properly modeled and incorporated in the force analysis. A comparison of the angular acceleration are shown in Figs. 8.33-8.36. The magnitude is not necessarily reduced in order to attenuate the link deflection.

Some of the problems faced during the experimental program are discussed here. The dynamic responses of the experimental work were often disturbed by unknown sources of electromagnetic noise and the results are not precisely repeatable. Thus, it was necessary to take several data sets for the same speed and select the best curve after first eliminating the noise disturbance by digital filtering. The operating speed does not always remain constant (variations of  $\pm 1$  rpm does exist), and this created a major problem in controlling the shaker motion, which is triggered by the zero crank-angle configuration pulse. The shaker/slider motion must be carefully orchestrated relative to the crank input.

In order to attenuate the vibrational amplitude of the rocker link to zero, a larger slider motion may be necessary. The procedure described below will yield a shaker/slider waveform which is different from the synthesized curve.

(1) Obtain the quasi-static response of the four-bar linkage.

Let  $w$  be the solution.



- (2) Let the quasi-static response in the Hill's equation (3.38) be the known variable, denoted by  $w'$ .

Let  $w' = -w$

- (3) Solve for the unknown variable  $\ddot{\ell}_t$ , which is shaker acceleration.
- (4) Integrate the solution obtained in step (3) to get the shaker/slider waveform.

The above procedure yielded a shaker amplitude of approximately 10 cm. This large amplitude is beyond the constraint imposed on the slider motion. Furthermore, a large shaker amplitude will change the configuration of the mechanism under investigation.

## CHAPTER 10

### CONCLUSIONS

A methodology has been proposed to reduce the vibrational response of a linkage mechanism at various operating speeds. A variational theorem has been developed and has been shown to provide a viable basis for establishing the governing equations of motion for predicting the response of a flexible rocker link of a four-bar linkage mechanism. An additional input to the prismatic joint of a four-bar linkage has shown to reduce the vibrational response of the rocker link. The waveform for the additional input was synthesized by analysing the response profile of the flexible link. The analytical model can be further improved by incorporating the structural damping of the member. The stability analysis of the system has provided a wide spectrum of stable region. Computer simulations provide a conservative prediction for the elastodynamic response, hence this model could be used with confidence in an industrial computer-aided design environment for the design of high-speed mechanism systems and robotic manipulators.

## **CHAPTER 11**

### **FUTURE WORK**

A philosophy directed towards developing computer-controlled intelligent machinery would be more practical for an industrial oriented environment. Clearly more work must be undertaken to document the control algorithm, whereby a microprocessor for instance would post-process the rocker link's response data to synthesize shaker/slider waveform which will provide an additional input to the linkage mechanism by exciting the electrodynamic shaker. This requires a careful orchestration of the crank motion and slider motion.

## **BIBLIOGRAPHY**

## BIBLIOGRAPHY

1. A. G. Erdman and G. N. Sandor, "Kineto-Elasto-Dynamics -A Review of State of Art and Trends", Mechanism and Machine Theory, Vol. 7, pp. 19-33, 1972.
2. G. G. Lowen and W. G. Jandrasits, "Survey of Investigation into the Behaviour of Mechanisms Containing Links with Distributed Mass and Elasticity", Mechanism and Machine Theory, Vol. 7, pp. 3-17, 1972.
3. A. G. Erdman, G. N. Sandor and R. G. Oakberg, "A General Method for Kineto-Elastodynamic Analysis of Mechanisms", ASME Journal of Engineering for Industry, Vol. 94B, pp. 1193-1205, 1972.
4. W. L. Cleghorn, R. G. Fenton and B. Tabarrok, "Optimum Design of High-Speed Flexible Mechanisms", Mechanism and Machine Theory, Vol. 16, pp. 399-406, 1981.
5. I. Imam and G. N. Sandor, "High Speed Mechanism Design -A General Analytical Approach", ASME Journal of Engineering for Industry, Vol. 97, pp. 609-628, 1975.
6. M. R. Khan, K. D. Willmert and W. A. Thornton, "Automated Analysis and Design of High-Speed Planar Mechanisms", Proceedings of the 5th OSU Applied Mechanisms Conference, Oklahoma City, Oklahoma, 1977.
7. W. A. Thornton, K. D. Willmert and M. R. Khan, "Mechanism Optimization via Optimality Criterion Techniques", ASME Journal of Mechanical Design, Vol. 101, pp. 392-397, 1979.
8. Ce. Zhang and H. T. Grandin, "Optimum Design of Flexible Mechanisms", ASME Journal of Mechanisms, Transmissions, and Automation in Design, Vol. 105, pp. 267-272, 1983.
9. C. K. Sung and B. S. Thompson, "Material-Selection: An Important Parameter in the Design of High-Speed Linkages", Mechanism and Machine Theory, Vol. 19, No. 4/5, pp. 389-396, 1984.
10. C. K. Sung, B. S. Thompson, P. Crowley and J. Cuccio, "An Experimental Study to Demonstrate The Superior Response Characteristics of Mechanisms Constructed with Composite Laminates", Mechanism and

Machine Theory, in press, May 1985.

11. B. S. Thompson and M. V. Ghandi, "The Finite Element Analysis of Mechanism Components made from Fiber-Reinforced Composite Materials", ASME paper No. 80-DET-63, 1980.

12. B. S. Thompson and C. K. Sung, "A Variational Formulation for the Dynamic Viscoelastic Finite Element Analysis of Robotic Manipulators Constructed from Composite Materials", ASME Journal of Mechanisms, Transmissions, and Automation in Design, Vol. 106, NO. 2, pp. 183-190, 1984.

13. H. Asada and P. I. Ro, "A Linkage Design for Direct-Drive-Robotic Arms", ASME Journal of Mechanisms, Transmissions, and Automation in Design, Vol. 107, pp. 536-540, Dec. 1985.

14. H. Asada and K. Youce-Toumi, "Analysis and Design of Semi-Direct-Drive Arm", Proceedings of the ACC, San Francisco, June 1983.

15. G. G. Lowen and C. Chassapis, "The Elastic Behavior of Linkages : An Update", Mechanism and Machine Theory, Vol. 21, No.1, pp. 33-42, 1986.

16. J. H. Oliver, D. A. Wysocki and B. S. Thompson, "The Synthesis of Flexible linkage by balancing the Tracer Point Quasi-Static Deflection's using Microprocessor and Advanced Materials Technologies", Mechanism and Machine Theory, Vol. 20, No. 2, pp. 103-114, 1985.

17. B. S. Thompson, K. Soong and C. K. Sung, "An Experimental Bread-Board Model For a Class of Intelligent High-Speed Machinery: some Preliminary results", Proceedings of the 9th OSU Applied Mechanisms Conference, Kansas City, Vol. II, pp. IV-1 to IV-4, Oct. 1985.

18. C. S. Hsu and W. H. Cheng, "Steady-State Response of a Dynamical System under Combined Parametric and Forcing Excitation", ASME Journal of Applied Mechanics, Vol. 41, pp. 371-378, 1974.

19. M. R. Smith and L. Maunder, "Inertia Forces in a Four-Bar Linkage", Journal of Mechanical Engineering Science, Vol. 9, pp. 218-225, 1967.

20. B. S. Thompson, "An Elastodynamic Analysis of Planar Linkage Mechanisms", Doctoral Dissertation , University of Dundee, Scotland, 1976.

21. B. S. Thompson and A. D. S. Barr, "A Variational Principle for the Motion of Components of Elastic Mechanisms", Proceedings of the Fourth World Congress on the Theory of Machines and Mechanisms, Newcastle-Upon-Tyne, U.K., Paper No. 43, 1975.

22. B. S. Thompson and R. P. Ashworth, "Resonance in Planar Linkage Mechanisms Mounted on Vibrating Foundations", Journal of Sound and Vibration, Vol. 49, No. 3, pp. 403-414, 1976.

23. V. V. Bolton, "The Dynamic Stability of Elastic Systems", San Francisco: Holden-Day, 1964.

24. R. E. D. Bishop and D. C. Johnson, "The Mechanics of Vibration", Cambridge University Press, pp. 318-320, 1960.

25. C.T. Chen, "Linear System Theory and Design", CBS, New York, pp. 51-53, 1984.

26. P. Hartman, "Ordinary Differential Equations", Wiley, New York, 1964.

27. Ling Dynamic Systems, Instruction Manual for Vibrator model 400 Series.